Contribution from the Department of Chemistry, University of Houston, Houston, Texas 77005, Laboratoire du Chimie du Solide et Inorganique Moléculaire, URA 254, Université de Rennes I, 35042 Rennes Cedex, France, and Department of Chemistry, Rice University, Houston, Texas 77251

Capping Considerations in Main-Group/Transition-Metal Clusters: Synthetic, Structural, and Theoretical Discussions of $[E_2Co_4(CO)_{10}(\mu\text{-}CO)]^{-/2-}$ (E = Sb, Bi)

Thomas A. Albright,*[†] Kyeong Ae Yee,[†] Jean-Yves Saillard,*[‡] Samia Kahlal,[‡] Jean-François Halet,[‡] J. S. Leigh,[§] and Kenton H. Whitmire*[§]

Received September 18, 1990

Unstable $SbCo_3(CO)_{12}$ (**1a**) is generated from the reaction of $SbCl_3$ and $Na[Co(CO)_4]$ in acidified aqueous solution. The compound decomposes under a variety of conditions to give varying mixtures of $[Sb_2Co_4(CO)_{10}(\mu\text{-}CO)]^-$ ([**2a**]$^-$), $[Sb_2Co_4(CO)_{10}(\mu\text{-}CO)]^{2-}$ ([**2a**]$^{2-}$), and $[Co(CO)_4]^-$. The two antimony–cobalt cluster compounds have been isolated as $[Et_4N]^+$ or $[PPN]^+$ salts. X-ray analyses show them to be isostructural with a tetrahedral Co_2Sb_2 core capped on the two $CoSb_2$ faces with $Co(CO)_3$ groups. [PPN][**2a**]: orthorhombic space group *Pbca* with a = 18.408 (3) Å, b = 33.038 (7) Å, c = 16.301 (3) Å, V = 9914 (3) Å^3, Z = 8, R = 0.053, R_w = 0.063. [PPN][**2a**]: triclinic space group $P\bar{1}$ with a = 15.618 (3) Å, b = 19.333 (4) Å, c = 15.124 (3) Å, α = 93.44 (2)°, β = 113.66 (2)°, γ = 69.60 (1)°, Z = 2, V = 3903 (2) Å^3, R = 0.045, R_w = 0.057. Cluster anions with the same formulation but with bismuth replacing antimony, [**2b**]$^-$ and [**2b**]$^{2-}$, are not generated in the same fashion but can be accessed by the reduction of $BiCo_3(CO)_9$ with cobaltocene. $[Cp_2Co][$**2b**$]$ has been characterized by single-crystal X-ray analysis: orthorhombic space group *Pbcn* with a = 14.973 (4) Å, b = 12.662 (4) Å, c = 14.671 (4) Å, Z = 4, V = 2782 (2) Å^3, R = 0.051, R_w = 0.066. Both [**2a**]$^-$ and [**2b**]$^-$ are paramagnetic with ESR signals found at g = 2.032 and 2.107, respectively. The mono- and dianions are related to each other by chemically and electrochemically reversible 1e redox cycles: $E_{1/2}$ = −0.54 V (Sb), −0.61 V (Bi). Considering the E–E interactions, the three compounds in this study are electron rich and violate normal electron counting rules. Molecular orbital calculations at the extended Hückel level were carried out on these molecules, as well as related derivatives. It is shown that the molecules can be regarded as either pentagonal bipyramids or bicapped tetrahedra. In both derivations the extra electrons enter into skeletal nonbonding or weakly antibonding molecular orbitals. The favored electron counts for other skeletal isomers and derivatives are determined and compared to experiment.

Introduction

Clusters have inspired a large body of work aimed at understanding the structures and associated bonding patterns.[1-5] The classic Wade's rules[1] as originally presented and as extended by Mingos[3] do much for rationalizing bonding and predicting structures of simple cluster molecules. When systems become complicated, however, numerous exceptions to these rules can be found. Attempts have been made to understand the exceptions. One such approach has been the application of graph theory by King,[5] who finds areas of localized and delocalized bonding within the cluster framework. Teo[4] has recently published some intriguing papers based on the application of Euler's theorem to Wade's rules and has developed a series of equations that allow for certain differences in electron count for a given structural type. More recently, exceptions have been found in mixed main-group/transition-metal cluster compounds where the bonding requirements (electronegativity and overlap) of the two different types of elements are quite dissimilar. Several reviews have appeared discussing the chemistry of this hybrid class.[6]

We recently discovered[7] two new antimony–cobalt carbonylates, $[Sb_2Co_4(CO)_{10}(\mu\text{-}CO)]^{-/2-}$, which were related by a reversible, one-electron redox cycle. The metal core appeared to be best described as a bicapped tetrahedral structure on the basis of bonding parameters found from X-ray structure analyses. The electron counts for both, however, are higher than expected and led us to undertake molecular orbital calculations to understand how the bonding of these complexes is related to the established theories. These results show a surprising similarity to those we found earlier for $[Bi_4Fe_4(CO)_{13}]^{2-}$ and suggest some general features of capping in clusters of this type, as well as an alternative way to view this cluster. This paper presents the full details of investigations reported in a preliminary communication.[7]

Experimental Section

General Methods. Unless otherwise specified, all synthetic manipulations were performed either with a vacuum line or under an atmosphere of purified nitrogen or argon by employing standard drybox or Schlenk-type inert-atmosphere techniques. Filtrations utilized medium-porosity Schlenk-type fritted filters. All solvents were distilled from appropriate drying agents[8] and were bubbled with nitrogen or argon for 30 min before use. Infrared spectra were obtained by using either a Perkin-Elmer 1430 ratio-recording infrared spectrophotometer or a Perkin-Elmer 1640 Fourier transform infrared spectrophotometer. Except for $SbCl_3$ (Alfa Products), which was sublimed before use, all materials were used as obtained: $Co_2(CO)_8$, Cp_2Co, anhydrous $BiCl_3$ (Strem Chemicals, Inc.); $SbCl_5$ (99%) (Alfa Products); $[Et_4N]Br$ (98%) (Aldrich Chemical Co., Inc.). $[PPN]Cl$,[9] $[Cu(MeCN)_4][BF_4]$[10] and $Bi[Co(CO)_4]_3$ (**1b**),[11] and $BiCo_3(CO)_9$[12] were prepared by literature methods.

Table I. Selected Infrared Spectral Data

compd	solvent	IR: ν_{CO}, cm^{-1}
1	hexane	2105 (w), 2080 (s), 2024 (ms), 2016 (ms), 2000 (mw), 1970 (sh)
$[Et_4N]$[**2a**]	THF	2010 (s), 1995 (ms), 1975 (m), 1802 (w)
$[PPN]_2$[**2b**]	CH_2Cl_2	1975 (s), 1950 (ms), 1925 (m), 1740 (w)
[PPN][**2b**]	Et_2O	1999 (s), 1987 (ms), 1968 (m), 1799 (w)
$[Cp_2Co]_2$[**2b**]	MeCN	1954 (s), 1940 (ms), 1915 (m), 1736 (w)

[†] University of Houston.
[‡] Université de Rennes I.
[§] Rice University.

(1) (a) Wade, K. *Adv. Inorg. Chem. Radiochem.* **1976**, *18*, 1. (b) Wade, K. *J. Chem. Soc., Chem. Commun.* **1971**, 792.
(2) Albright, T. A.; Burdett, J. K.; Whangbo, M.-H. *Orbital Interactions in Chemistry*; John Wiley & Sons: New York, 1985.
(3) (a) Mingos, D. M. P. *Nature (London), Phys. Sci.* **1972**, *236*, 99. (b) Mingos, D. M. P. *Acc. Chem. Res.* **1984**, *17*, 311. (c) Mingos, D. M. P.; Forsyth, M. I. *J. Chem. Soc., Dalton Trans.* **1977**, 610. (d) Mingos, D. M. P. *J. Chem. Soc., Chem. Commun.* **1983**, 706. (e) Johnston, R. L.; Mingos, D. M. P. *J. Organomet. Chem.* **1985**, *280*, 407. (f) Johnston, R. L.; Mingos, D. M. P. *J. Organomet. Chem.* **1985**, *280*, 419.
(4) (a) Teo, B. K. *Inorg. Chem.* **1984**, *23*, 1251. (b) Teo, B. K.; Longoni, G.; Chung, F. R. K. *Inorg. Chem.* **1984**, *23*, 1257. (c) Teo, B. K. *Inorg. Chem.* **1985**, *24*, 1627. (d) Teo, B. K. *Inorg. Chem.* **1985**, *24*, 4209.
(5) (a) King, R. B.; Rouvray, D. H. *J. Am. Chem. Soc.* **1977**, *99*, 7834. (b) King, R. B. *Inorg. Chim. Acta* **1986**, *116*, 99. (c) King, R. B. *Inorg. Chim. Acta* **1986**, *116*, 119. (d) King, R. B. *Inorg. Chim. Acta* **1986**, *116*, 125.
(6) (a) Whitmire, K. H. *J. Coord. Chem.* **1988**, *17*, 95. (b) Norman, N. C. *Chem. Soc. Rev.* **1988**, *17*, 269. (c) Herrmann, W. A. *Angew. Chem., Int. Ed. Engl.* **1986**, *25*, 56. (d) Huttner, G.; Knoll, K. *Angew. Chem., Int. Ed. Engl.* **1987**, *26*, 743.
(7) (a) Leigh, J. S.; Whitmire, K. H.; Yee, K. A.; Albright, T. A. *J. Am. Chem. Soc.* **1989**, *111*, 2726. (b) The cluster dianion [**2a**]$^{2-}$ has been independently prepared: Martinengo, S.; Ciani, G. Personal communication.
(8) Gordon, A. J.; Ford, R. A. *The Chemist's Companion*; John Wiley & Sons: New York, 1972; p 445.
(9) Ruff, J. K.; Schlientz, W. D. *Inorg. Synth.* **1975**, *15*, 84.
(10) Himmereich, P.; Sigwarth, C. *Experientia* **1963**, *19*, 488.

0020-1669/91/1330-1179$02.50/0

Sodium naphthalenide was prepared by vacuum-distilling THF into a flask kept at −196 °C that contained 1 equiv each of sublimed sodium metal and naphthalene. The flask and its contents were then warmed to room temperature to allow the reaction to occur, forming the green sodium naphthalenide/THF solution. Elemental analyses were performed by Galbraith Laboratories, Inc., Texas Analytical Laboratories, Inc., or Desert Analytics. All yields reported are with respect to the main-group element used in the reaction unless otherwise specified. Infrared data are provided in Table I.

Synthesis of $Sb[Co(CO)_4]_3$ (1a). Addition of $SbCl_3$ (0.595 g, 2.60 mmol) to 30 mL of H_2O produced a white precipitate of antimony oxyhalide, which was acidified by dropwise addition of concentrated HCl until all of the precipitate redissolved. Approximately 8 mL of 1% Na/Hg amalgam was added to $Co_2(CO)_8$ (1.337 g, 3.910 mmol) in THF (50 mL), and the mixture was stirred several hours. After the THF solution was filtered through Celite, the solvent was removed under vacuum. The $Na[Co(CO)_4]$ was redissolved in H_2O (30 mL), and the solution was added by syringe to the stirred antimony halide solution. The solution was stirred 1 h, during which time a dark green precipitate formed. The precipitate was isolated by filtration, washed with three 20-mL portions of H_2O, and dried under vacuum to give **1a** (1.05 g, 1.65 mmol, 63% yield).

Synthesis of $[Et_4N][Sb_2Co_4(CO)_{10}(\mu\text{-}CO)]$ ($[Et_4N][2a]$). Compound **1a** (0.51 g, 0.80 mmol) and $[Et_4N]Br$ (0.25 g, 1.2 mmol) were placed together in a Schlenk flask with a magnetic stir bar. THF (60 mL) was added by syringe and the solution stirred overnight to form $[Et_4N][2a]$ and $[Et_4N][Co(CO)_4]$ as evidenced by infrared spectroscopy. The solution was filtered from insoluble material, and the solvent was removed under vacuum. After the residue was washed with MeOH (20 mL) to remove $[Et_4N][Co(CO)_4]$ and excess $[Et_4N]Br$, the remaining solid was dissolved in THF (40 mL), the solution was filtered, and the filtrate was layered with hexane (60 mL) at room temperature to recrystallize $[Et_4N][2a]$ (0.16 g, 0.17 mmol, 43% yield). Anal. Calcd for $Sb_2Co_4C_{19}O_{11}NH_{20}$: C, 24.87; H, 2.20; N, 1.53. Found: C, 24.90; H, 2.35; N, 1.70.

Synthesis of $[Et_4N]_2[Sb_2Co_4(CO)_{10}(\mu\text{-}CO)]$ ($[Et_4N]_2[2a]$). A 1-equiv amount of sodium naphthalenide (0.17 mmol) in 1 mL of THF was added to a solution of $[Et_4N][2a]$ (0.155 g, 0.169 mmol) in 20 mL of THF and the resultant solution stirred 30 min to form $[2a]^{2-}$ along with some $[Co(CO)_4]^-$. Solid $[Et_4N]Br$ (0.05 g, 0.24 mmol) was added and stirring was continued for 1 h more. The solution was filtered from unreacted $[Et_4N]Br$, and the solvent was removed under vacuum. $[Et_4N][2a]$ may be recrystallized from THF/hexane, but the compound is very easily oxidized and it is difficult to obtain in pure form.

Isolation of $[PPN][2a]$ and $[PPN]_2[2a]$ from the Decomposition of 1a in THF. Compound **1a** (0.363 g, 0.572 mmol) was stirred in THF (40 mL) for several hours, forming a dark precipitate, which was then isolated by filtration. After this precipitate was stirred with [PPN]Cl (0.50 g) in MeCN (30 mL) overnight, the solution that resulted was filtered from insoluble material and the solvent removed under vacuum. The residue was then redissolved in CH_2Cl_2 (15 mL), and the solution was layered with MeOH (30 mL) at room temperature. Upon standing, a precipitate formed composed of brown powder and a few brown crystals. X-ray analysis of one of the crystals determined the structure to be that of $[PPN]_2[2a]$. The solvent of the supernatant was then removed under vacuum. Et_2O (20 mL) was stirred with the solid residue to extract $[PPN][2a]$ from $[PPN][Co(CO)_4]$ and unreacted [PPN]Cl. The green Et_2O solution was filtered, concentrated to about half-volume, and layered with hexane (15 mL), giving X-ray-quality crystals of $[PPN][2a]$ (0.020 g, 0.015 mmol, 5% yield).

Reaction of 1a with $[Cp_2Co][Co(CO)_4]$. $Co_2(CO)_8$ (0.072 g, 0.21 mmol) and Cp_2Co (0.080 g, 0.42 mmol) were mixed together in a Schlenk flask with a magnetic stir bar. CH_2Cl_2 (40 mL) was added by syringe, and the solution was stirred 2 h, forming $[Cp_2Co][Co(CO)_4]$. This solution was filtered onto solid **1a** (0.263 g, 0.414 mmol) and stirred another 4 days. Monitoring the reaction with infrared spectroscopy showed little of the added $[Cp_2Co][Co(CO)_4]$ to react. A dark precipitate that formed during the reaction was isolated by filtration and redissolved in MeCN (20 mL). An infrared spectrum of this solution showed bands corresponding to $[2a]^-$, $[2a]^{2-}$, and $[Co(CO)_4]^-$.

Reaction of 1a with Cp_2Co. Compound **1a** (0.49 g, 0.77 mmol) and Cp_2Co (0.15 g, 0.79 mmol) were mixed together in a Schlenk flask containing a magnetic stirring bar. CH_2Cl_2 (60 mL) was added by syringe, and the solution was stirred 5 days. A dark precipitate and $[Co(CO)_4]^-$ formed during that time. After the precipitate was isolated by filtration, [PPN]Cl (0.45 g) in MeCN (20 mL) was added to the solid, and the mixture was stirred overnight. An infrared spectrum of the MeCN solution then showed IR bands corresponding to small amounts of $[2a]^-$ and $[2a]^{2-}$ and a large amount of $[Co(CO)_4]^-$.

Reaction of $SbCl_5$ with $Na[Co(CO)_4]$ (1:4 Ratio). $SbCl_5$ (0.25 mL, 0.58 g, 1.9 mmol) was added by syringe to a stirred THF (70 mL) solution of $Na[Co(CO)_4]$, which had been prepared from the Na/Hg analgam reduction of $Co_2(CO)_8$. After the solution was stirred for 2 days, the only carbonyl product observable by infrared spectroscopy in the green solution was $[2a]^-$. The solution was then filtered from insoluble material and the solvent removed under vacuum to isolate $[Na(THF)_x][2a]$ (1.2 g), which could be converted to the $[PPN]^+$ salt by cation exchange in THF.

In Situ Chemical Reduction/Oxidation of $[PPN][2a]$. Cp_2Co (2 mg, 1×10^{-5} mol) in 2 mL of CH_2Cl_2 was added by syringe in a stirred solution of $[PPN][2a]$ (13 mg, 9.8×10^{-6} mol) in 5 mL of CH_2Cl_2. The resulting solution was stirred 30 min, forming $[2a]^{2-}$ as identified by infrared spectroscopy. $[Cu(MeCN)_4][BF_4]$ (4 mg, 1×10^{-5} mol) in 2 mL of CH_2Cl_2 was then added and the solution stirred another 20 min, cleanly re-forming $[2a]^-$.

Synthesis of $[PPN][Bi_2Co_4(CO)_{10}(\mu\text{-}CO)]$ ($[PPN][2b]$). A 1-equiv amount of sodium naphthalenide (0.79 mmol) in 1 mL of THF was added by syringe to a stirred solution of $BiCo_3(CO)_9$ (**3**; 0.504 g, 0.790 mmol) in 60 mL of THF. After being stirred for 30 min, the solution was filtered and the solvent removed under vacuum. The solid residue was washed with three 40-mL portions of hexane to remove unreacted starting material and naphthalene and then dissolved in 40 mL of MeOH. A solution of [PPN]Cl (0.45 g) in 10 mL of MeOH was added and the solution stirred 30 min. It was then filtered and the solvent removed under vacuum. Et_2O (60 mL) was added to the solid, and the mixture was stirred several minutes to extract $[PPN][2b]$ from $[PPN][Co(CO)_4]$, [PPN]Cl, and NaCl. The Et_2O solution was filtered, concentrated to about two-thirds volume, and layered with hexane (70 mL) at room temperature to precipitate brown crystals of $[PPN][2b]$ (0.36 g, 0.24 mmol, 61% yield). ESR spectrum of $[PPN][2a]$ in THF: $T = 12$ K, $n = 9.2880$ GHz, $H_0 = 3265$ G, $g = 2.032$.

Synthesis of $[Cp_2Co][Bi_2Co_4(CO)_{10}(\mu\text{-}CO)]$ ($[Cp_2Co][2b]$). **1b** (0.303 g, 0.475 mmol) and Cp_2Co (0.089 g, 0.47 mmol) were mixed together in a Schlenk flask. CH_2Cl_2 (30 mL) was added by syringe, and the solution was stirred about 30 min, forming $[Cp_2Co][2b]$ and $[Cp_2Co][Co(CO)_4]$. After filtration, the solvent was removed under vacuum and the resulting solid residue was washed with five 15-mL portions of toluene to remove unreacted starting material. The product was then redissolved in a minimal amount of CH_2Cl_2 and the solution cooled to −30 °C overnight, during which time brown crystals of $[Cp_2Co][2b]$ (0.089 g, 0.077 mmol, 32% yield) formed. Anal. Calcd for $Bi_2Co_5C_{21}O_{11}H_{10}$: Bi, 36.31; Co, 25.60. Found: Bi, 31.93; Co, 25.00. ESR spectrum of $[Cp_2Co][2b]$ in CH_2Cl_2: $T = 12$ K, $n = 9.2887$ GHz, $H_0 = 3150$ G, $g = 2.107$.

Synthesis of $[Cp_2Co]_2[2b]$. Compound **1b** (0.175 g, 0.274 mmol) and Cp_2Co (0.053 g, 0.28 mmol) were mixed together in a Schlenk flask. CH_2Cl_2 (20 mL) was added by syringe, and the solution was stirred 1 h, forming $[Cp_2Co][2b]$ and $[Cp_2Co][Co(CO)_4]$. Another 0.051 g of Cp_2Co (0.27 mmol) in 10 mL of CH_2Cl_2 was added and the solution stirred another 1.5 h. $[Cp_2Co]_2[2b]$ precipitated as the reaction progressed. The brown solid was isolated by filtration, washed with two 20-mL portions of CH_2Cl_2, dried under vacuum, and recrystallized from acetone or acetone/hexane (62 mg, 0.046 mmol, 34% overall yield). Anal. Calcd for $Bi_2Co_6C_{31}O_{11}H_{20}$: Bi, 31.39; Co, 26.39; C, 27.79. Found: Bi, 28.03; Co, 22.15; C, 23.16.

Synthesis of $[PPN]_2[2b]$. A 1-equiv amount of sodium naphthalenide (0.017 mmol) in 1 mL of THF was added by syringe to a stirred solution of $[PPN][2b]$ in 30 mL of THF. After being stirred for 30 min, the solution was filtered and the solvent removed under vacuum. The solid residue was washed with two 20-mL portions of hexane to remove naphthalene. After being dried under vacuum, the solid was redissolved in MeOH (15 mL). [PPN]Cl (0.10 g, 0.17 mmol) in MeOH (10 mL) was added by syringe with stirring to precipitate $[PPN]_2[2b]$. The brown solid was isolated by filtration, washed with two 20-mL portions of MeOH, and dried under vacuum.

Cyclic Voltammetry. Cyclic voltammetry measurements were obtained by using a Bioanalytical Systems Inc. CV-27 voltammograph with a Bioanalytical Systems Inc. C-1B cell stand and a Bausch and Lomb Houston Instrument Division 100 XY recorder. CH_2Cl_2, which was distilled from P_4O_{10}, was bubbled with nitrogen or argon before use. The supporting electrolyte solution, 0.1 M $[n\text{-}Bu_4N][ClO_4]$ in CH_2Cl_2, was prepared fresh before each series of measurements. All compound manipulations prior to voltammetry measurements were performed by using standard inert-atmosphere techniques. Compound/electrolyte solutions also were bubbled with nitrogen or argon in the CV cell before the

(11) Etzrodt, G.; Boese, R.; Schmid, G. *Chem. Ber.* **1979**, *112*, 2574.
(12) (a) Whitmire, K. H.; Leigh, J. S.; Gross, M. E. *J. Chem. Soc., Chem. Commun.* **1987**, 926. (b) Martinengo, S.; Ciani, G. *J. Chem. Soc., Chem. Commun.* **1987**, 1589.

Table II. Selected Crystal Data for Compounds [PPN][**2a**], $[PPN]_2$[**2a**], and $[Cp_2Co]$[**2b**]

	[PPN][**2a**]	$[PPN]_2$[**2a**]	$[Cp_2Co]$[**2b**]
chem formula	$C_{47}Co_4H_{30}NO_{11}P_2Sb_2$	$C_{83}Co_4H_{60}N_2O_{11}P_4Sb_2$	$Bi_2C_{21}Co_5H_{10}O_{11}$
fw	1325.93	1864.52	1150.93
system	orthorhombic	triclinic	orthorhombic
space group	*Pbca* (No. 61)	$P\bar{1}$ (No. 2)	*Pbcn* (No. 60)
a, Å	18.408 (3)	15.618 (3)	14.973 (4)
b, Å	33.038 (7)	19.333 (4)	12.662 (4)
c, Å	16.301 (3)	15.124 (3)	14.671 (4)
α, deg		93.44 (2)	
β, deg		113.66 (2)	
γ, deg		69.60 (1)	
V, Å^3	9914 (3)	3903 (2)	2782 (2)
Z	8	2	4
T, °C	−80	23	23
R	0.053	0.046	0.051
R_w	0.063	0.057	0.066

experiment, and measurements were taken with a blanket of inert gas over the solution. Cyclic voltammographs were obtained at room temperature of approximately 1 mM solutions of cluster complexes in 0.1 M $[n\text{-}Bu_4N][ClO_4]/CH_2Cl_2$ by using a Ag/AgCl reference electrode, a glassy-carbon working electrode, and a platinum auxiliary electrode. For comparison purposes, a cyclic voltammogram of ferrocene performed under similar conditions showed a reversible oxidation wave at $E_{1/2}$ = 0.48 V (scan rate = 40 mV/s, ΔE_p = 100 mV, i_{pa}/i_{pc} = 1.05).

X-ray Crystallography. General Methods. X-ray crystallographic data were collected via TEXSAN[13] data collection software on a Rigaku AFC5S automated four-circle diffractometer using graphite-monochromated Mo Kα radiation (λ = 0.7107 Å). The crystals were mounted on the tips of glass fibers by using epoxy cement. Unit cell parameters were determined from the least-squares best fit of 25 reflections ($6 \le 2\theta \le 18°$). Three standards were measured every 150 reflections. The data were collected by using 2θ–ω scans and corrected for absorption (ψ scans) and Lorentz–polarization effects. In the case of $[PPN]_2$[**2b**], the data were also corrected for an 8.2% linear decay. Least-squares refinement minimized $\sum w(|F_o| - |F_c|)^2$, $w = [\sigma^2(F_o)]^{-1}$ (σ^2 = variance), for all compounds.[14] Selected crystallographic data collection parameters are listed in Table II. A more complete listing is provided in the supplementary material.

Crystal Data Collection and Structure Solution for [PPN][2a]. Black needlelike crystals of the compound grew overnight from an Et_2O solution layered with hexane at room temperature. Systematic absences unambiguously indicated the centrosymmetric space group *Pbca* (No. 61). The structure was solved with the direct-methods program MITHRIL (4.1.0),[15] which located the antimony and cobalt atoms of the anion. Initial difference Fourier syntheses using the TEXSAN (2.0)[13] structure analysis package located the nitrogen and phosphorus atoms of the cation. The structure was expanded by using the phase refinement and extension program DIRDIF,[16] which located most of the carbon atoms on the phenyl rings and some of the carbonyl carbon and oxygen atoms. Further difference Fourier syntheses located all remaining non-hydrogen atoms. Idealized hydrogen atom positions on the phenyl rings of the $[PPN]^+$ cation were calculated. Full-matrix least-squares refinement proceeded with the phenyl rings of the cation defined as rigid bodies and refined with each atom having an individual isotropic B(eq) value. All other atoms were refined anisotropically. Refinement converged with R = 0.053, R_w = 0.063, $(\Delta/\sigma)_{max}$ = 0.03, $(\Delta\rho)_{max}$ = 0.79 e/Å^3, number of observations = 3729, number of variables = 352, and S = 1.20.

Crystal Data Collection and Structure Solution for $[PPN]_2$[2a]. Black platelike crystals of the compound grew overnight from a CH_2Cl_2 solution layered with methanol at room temperature. Intensity statistics indicated a centrosymmetric space group, and successful solution and refinement proved $P\bar{1}$ (No. 2) to be the correct choice. The structure was solved by using the direct-methods program in SHELXS86,[17] which located the antimony and cobalt atoms of the anion. Initial difference Fourier syntheses using the TEXSAN (2.0)[13] structure analysis package located a phosphorus atom on each of the cations. The structure was expanded by using the phase refinement and extension program DIRDIF,[16] which located much of the remaining structure. Further difference Fourier syntheses located all remaining non-hydrogen atoms. Idealized hydrogen atom positions on the phenyl rings of the $[PPN]^+$ cations were calculated. Full-matrix least-squares refinement proceeded with the phenyl rings of the $[PPN]^+$ cations defined as rigid bodies and refined with each atom having an individual isotropic B(eq) value. All other atoms were refined anisotropically. Refinement converged with R = 0.064 and R_w = 0.071 for $I > 3\sigma(I)$. Raising the σ cutoff to 6 gave final values of R = 0.046, R_w = 0.057, $(\Delta/\sigma)_{max}$ = 0.12, $(\Delta\rho)_{max}$ = 1.55 e/Å^3, number of observations = 3087, number of variables = 451, and S = 1.39.

Table III. Extended Hückel Parameters

	orbital	H_{ii}, eV	ζ_1	ζ_2	c_1[a]	c_2[a]
H	1s	−13.60	1.3			
C	2s	−21.40	1.625			
	2p	−11.40	1.625			
O	2s	−32.30	2.275			
	2p	−14.80	2.275			
P	3s	−18.6	1.6			
	3p	−14.0	1.6			
Bi	6s	−15.75	2.653			
	6p	−10.52	2.092			
Sb	5s	−18.8	2.323			
	5p	−11.7	1.999			
Co	4s	−9.21	2.0			
	4p	−5.29	2.0			
	3d	−13.18	5.55	1.90	0.5551	0.6461

[a] Coefficients in the double-ζ expansion.

Crystal Data Collection and Structure Solution for $[Cp_2Co]$[2b]. Brown prismatic crystals of the compound grew from a CH_2Cl_2 solution cooled at −30 °C overnight. Space group determination was difficult, as the weak data set led to ambiguous systematic absences in the *h0l* zone. Systematic absences and intensity statistics did, however, indicate four possible space group choices: Nos. 52, 56, 60, and 62. Trial and error determined *Pbcn* (No. 60) to be correct. After transformation to the standard setting (from *Pnca*, setting No. 3), the structure was solved by using the direct-methods program in SHELXS86,[17] which located the bismuth and cobalt atoms. Further difference Fourier syntheses using the TEXSAN (2.0) structure analysis package[13] located the carbon and oxygen atoms. Full-matrix least-squares refinement proceeded with the bismuth and cobalt atoms refined anisotropically and the carbon and oxygen atoms isotropically. Idealized hydrogen atom positions on the Cp rings of the cobaltocenium cation were not calculated. Refinement converged with R = 0.073 and R_w = 0.085 for $I > 3\sigma(I)$. Raising the σ cutoff to 5 gave final values of R = 0.051, R_w = 0.066, $(\Delta/\sigma)_{max}$ = 0.07, $(\Delta\rho)_{max}$ = 1.58 e/Å^3, number of observations = 693, number of variables = 98, and S = 1.54.

Theoretical Calculations. All computations were carried out within the extended Hückel method by using a modified Wolfsberg–Helmholz formula.[18] All bond distances and angles for the compounds were

(13) Molecular Structure Corp., The Woodlands, TX: CRYSTAN/TEXTL, (1987), program for data collection; CONTROL (1988), program for data collection; TEXSAN (1988), program package for crystal structure determination and refinement.
(14) Cromer, D. T.; Waber, J. T. *International Tables for X-ray Crystallography*; Kynoch Press: Birmingham, England, 1974; Vol. IV, pp 71 (scattering factors), 148 (anomalous dispersion). Present distributor Kluwer Academic Publishers, Dordrecht, The Netherlands.
(15) Gilmore, C. J. MITHRIL, an integrated direct methods program. *J. Appl. Crystallog.* **1984**, *17*, 42.
(16) Beurskens, P. T. DIRDIF, an automatic procedure for phase extension and refinement of difference structure factors; Technical Report 1984/1; Crystallography Laboratory: Toernooiveld, 6525 Ed Nijmegen, Netherlands.
(17) Sheldrick, G. M. SHELXS86 (1986), program for crystal structure determination.
(18) Hoffmann, R. *J. Chem. Phys.* **1963**, *39*, 1397. Ammeter, J. H.; Bürgi, H. B.; Thibeault, J. C.; Hoffmann, R. *J. Am. Chem. Soc.* **1978**, *100*, 3686.

derived from averaged values in X-ray structures.[7,12b,19] In all cases Co–C and C–O distances were fixed at 1.76 and 1.15 Å, respectively. For the hypothetical P_6^{6+} cluster a P–P distance of 2.10 Å was used. Table III lists the parameters used in the calculations.

Results

The reaction of $SbCl_3$ with $Na[Co(CO)_4]$ proceeds similarly to that of $BiCl_3$ and produces a precipitate whose infrared spectrum when taken immediately upon dissolution is almost identical with that of $Bi[Co(CO)_4]_3$ (**1b**). Unlike the bismuth compound,

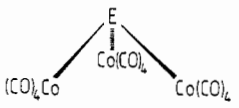

1a E = Sb
1b E = Bi

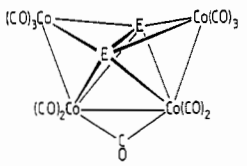

2a E = Sb
2b E = Bi

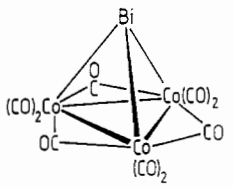

3

however, the antimony species is not stable and begins to decompose immediately upon dissolving in a variety of organic solvents. The products of decomposition were shown to include $[\mathbf{2a}]^-$, $[\mathbf{2a}]^{2-}$, and $[Co(CO)_4]^-$ by infrared spectroscopy and X-ray analyses (vide infra). The relative concentrations of these products depended upon the reaction conditions. The presence of $[Et_4N]Br$ promotes a cleaner reaction and apparently inhibits the formation of $[\mathbf{2a}]^{2-}$. When excess $[Co(CO)_4]^-$ was added in hopes of obtaining a stable $[Sb\{Co(CO)_4\}_4]^-$ anion similar to the known bismuth complex,[20] there was no noticeable effect on the decomposition reaction. Addition of Cp_2Co to **1a** promoted the formation of $[Co(CO)_4]^-$, but $[\mathbf{2a}]^-$ and $[\mathbf{2a}]^{2-}$ were formed as before. Treating $BiCo_3(CO)_9$ (**3**) with 1 equiv of cobaltocene of sodium naphthalenide causes molecular fragmentation and recombination to produce $[\mathbf{2b}]^-$ along with $[Co(CO)_4]^-$. In situ treatment of this product solution with $[Cu(MeCN)_4][BF_4]$ re-forms **3** along with $Co_4(CO)_{12}$.

The observation of both $[\mathbf{2a}]^-$ and $[\mathbf{2a}]^{2-}$ as products for the decomposition of **1a** prompted us to examine the obvious redox relationship between them and also to attempt reduction of the bismuth-containing compound. Both $[\mathbf{2a}]^-$ and $[\mathbf{2b}]^-$ may be reduced chemically by treatment with 1 equiv of cobaltocene or sodium naphthalenide to form their corresponding dianions. The infrared spectra of the Sb and Bi products are very similar qualitatively to that of the monoanion except that the frequencies are shifted to lower energy as expected. The dianion $[\mathbf{2b}]^{2-}$ is presumably isostructural with $[\mathbf{2a}]^-$, $[\mathbf{2a}]^{2-}$, and $[\mathbf{2b}]^-$ although attempts to obtain single-crystal data have not yet proven fruitful. Both the antimony and bismuth forms of $[\mathbf{2}]^{2-}$ are easily oxidized to the monoanions and are thus difficult to obtain in pure form. Stoichiometric addition of a mild oxidant such as $[Cu(NCMe)_4][BF_4]$ regenerates the monoanions. These qualitative observations are supported by cyclic voltammograms, which gave electrochemically reversible reduction waves at $E_{1/2} = -0.54$ V (scan rate = 20 mV/s, ΔE_p = 70 mV, i_{pa}/i_{pc} = 0.96) for [PPN][**2a**] and $E_{1/2} = -0.61$ V (scan rate = 20 mV/s, ΔE_p = 70 mV, i_{pa}/i_{pc} = 0.88) for [PPN][**2b**]. Compounds [PPN][**2a**] and $[Cp_2Co][\mathbf{2b}]$ show ESR spectra indicative of one unpaired electron. For both the signals are broad and no fine structure was resolved under the conditions studied.

Oxidation of [PPN][**2a**] shows a quasi-reversible oxidation wave at $E_{1/2} = +0.06$ V (scan rate = 50 mV/s, ΔE_p = 120 mV, i_{pa}/i_{pc} = 1.8). Further oxidation shows a large wave beginning at potentials greater than +0.6 V that peaks beyond the voltage ranged studied. Oxidation of [PPN][**2b**] was similar, giving a quasi-reversible oxidation wave at $E_{1/2} = +0.03$ V (scan rate = 20 mV/s, ΔE_p = 120 mV, i_{pa}/i_{pc} = 1.5–1.9), followed by a large, broad wave series occurring at voltages greater than +0.5 V. In neither case has it yet proven possible to observe stable oxidation products from these processes. In the case of $[\mathbf{2b}]^-$, chemical oxidation led to the isolation of **1b**, obviously arrived at by complicated fragmentation and rearrangement processes.

Crystal Structures of [PPN][2a], $[PPN]_2$[2a], and $[Cp_2Co]$[2b]. Single-crystal X-ray analyses performed on compounds [PPN][**2a**], $[PPN]_2$[**2a**], and $[Cp_2Co][\mathbf{2b}]$ showed the metal core of all three to be qualitatively the same; therefore, an ORTEP[21] diagram of only one of the anions ($[\mathbf{2a}]^{2-}$) is shown (Figure 1). Positional and isotropic displacement parameters are given in Tables IV–VI, and bond metricals, in Tables VII–XII. The core structure can best be described as a tetrahedron composed of two main group atoms and two cobalt atoms. Two terminal carbonyl ligands are attached to each of these cobalt atoms, and a bridging carbonyl lies along the Co–Co bond. $Co(CO)_3$ groups cap each of the two E_2Co (E = Sb, Bi) triangular faces of the parent tetrahedron.[7,12b]

The crystal structure of [PPN][**2a**] consists of ordered $[PPN]^+$ cations and $[\mathbf{2a}]^-$ anions in a 1:1 ratio, and the structure of $[PPN]_2$[**2a**] consists of ordered $[PPN]^+$ cations and $[\mathbf{2a}]^{2-}$ anions in a 2:1 ratio. The cations in both molecules are similar to other known $[PPN]^+$ salts, possess no unusual features, and will not be discussed.

The crystal structure of $[Cp_2Co][\mathbf{2b}]$ consists of ordered $[Cp_2Co]^+$ cations and $[\mathbf{2b}]^-$ anions in a 1:1 ratio. Like $[Cp_2Co][Bi\{Co(CO)_4\}_4]$, the Cp rings of the cation are staggered as in most standard cobaltocenium salts.[20] The anion has crystallographically imposed C_{2v} symmetry with the C_2 axis intersecting the midpoint between the two bismuth atoms and passing through the carbon and oxygen atoms of the bridging carbonyl.

Table IV. Positional Parameters and B(eq) Values for the Cluster Anion in [PPN][**2a**]

atom	x	y	z	B(eq), Å^2
Sb(1)	0.93996 (6)	0.14895 (3)	0.30053 (6)	2.71 (4)
Sb(2)	0.93525 (6)	0.09936 (3)	0.15302 (6)	2.67 (4)
Co(1)	0.8294 (1)	0.10390 (6)	0.2587 (1)	3.1 (1)
Co(2)	0.8668 (1)	0.16998 (6)	0.1679 (1)	2.5 (1)
Co(3)	1.0029 (1)	0.17154 (6)	0.1592 (1)	2.6 (1)
Co(4)	1.0502 (1)	0.10733 (6)	0.2459 (1)	3.2 (1)
O(1)	0.9238 (6)	0.2350 (3)	0.0720 (6)	3.8 (5)
O(11)	0.8732 (7)	0.0348 (4)	0.3596 (7)	5.4 (7)
O(12)	0.7290 (6)	0.0663 (4)	0.1431 (7)	5.1 (7)
O(13)	0.7317 (7)	0.1519 (4)	0.3636 (8)	6.2 (8)
O(21)	0.7654 (6)	0.1526 (3)	0.0342 (6)	4.2 (6)
O(22)	0.7814 (7)	0.2305 (3)	0.2584 (7)	5.4 (7)
O(31)	1.0916 (6)	0.1617 (4)	0.0118 (7)	5.4 (7)
O(32)	1.0966 (6)	0.2334 (3)	0.2301 (9)	6.4 (8)
O(41)	1.0375 (7)	0.0396 (4)	0.3599 (9)	6.5 (8)
O(42)	1.1341 (7)	0.0759 (4)	0.1069 (8)	5.8 (8)
O(43)	1.1474 (7)	0.1587 (4)	0.3377 (8)	5.5 (7)
C(1)	0.9337 (9)	0.2060 (4)	0.1137 (9)	3.2 (7)
C(11)	0.856 (1)	0.0625 (5)	0.319 (1)	3.7 (9)
C(12)	0.769 (1)	0.0817 (4)	0.186 (1)	3.8 (9)
C(13)	0.769 (1)	0.1343 (5)	0.322 (1)	3.7 (8)
C(21)	0.8053 (7)	0.1589 (4)	0.085 (1)	2.7 (7)
C(22)	0.815 (1)	0.2067 (5)	0.222 (1)	3.5 (8)
C(31)	1.055 (1)	0.1643 (5)	0.069 (1)	3.7 (8)
C(32)	1.0595 (9)	0.2087 (4)	0.204 (1)	3.4 (7)
C(41)	1.0413 (9)	0.0673 (5)	0.315 (1)	4 (1)
C(42)	1.102 (1)	0.0892 (5)	0.162 (1)	4 (1)
C(43)	1.109 (1)	0.1390 (6)	0.300 (1)	5 (1)

(19) Mason, R.; Thomas, K. M.; Mingos, D. M. P. *J. Am. Chem. Soc.* **1973**, *95*, 3802.
(20) (a) Leigh, J. S.; Whitmire, K. H. *Angew. Chem., Int. Ed. Engl.* **1988**, *27*, 396. (b) Martinengo, S.; Fumagalli, A.; Ciani, G.; Moret, M. *J. Organomet. Chem.* **1988**, *347*, 413.
(21) Johnson, C. K. ORTEPII; Report ORNL-5138; Oak Ridge National Laboratory: Oak Ridge, TN, 1976.

Table V. Positional Parameters and B(eq) Values for the Cluster Anion of $[PPN]_2$[**2a**]

atom	x	y	z	B(eq), Å^2
Sb(1)	0.1943 (1)	0.32683 (7)	0.1726 (1)	3.40 (9)
Sb(2)	0.3558 (1)	0.22120 (8)	0.3285 (1)	3.58 (9)
Co(1)	0.2452 (2)	0.3506 (2)	0.3585 (2)	3.7 (2)
Co(2)	0.1676 (2)	0.2437 (2)	0.2842 (2)	4.6 (2)
Co(3)	0.2496 (2)	0.1831 (1)	0.1624 (2)	3.8 (2)
Co(4)	0.3732 (2)	0.2553 (1)	0.1691 (2)	3.7 (2)
O(1)	0.119 (1)	0.1218 (8)	0.189 (1)	7 (1)
O(11)	0.390 (1)	0.421 (1)	0.387 (1)	7 (1)
O(12)	0.056 (1)	0.4745 (9)	0.298 (1)	6 (1)
O(13)	0.289 (1)	0.299 (1)	0.554 (1)	9 (1)
O(21)	−0.040 (1)	0.336 (1)	0.219 (1)	9 (1)
O(22)	0.213 (2)	0.157 (2)	0.458 (2)	15 (3)
O(31)	0.124 (1)	0.200 (1)	−0.041 (1)	9 (1)
O(32)	0.407 (1)	0.0380 (9)	0.204 (1)	8 (1)
O(41)	0.400 (1)	0.397 (1)	0.170 (1)	8 (1)
O(42)	0.574 (1)	0.147 (1)	0.261 (1)	10 (1)
O(43)	0.313 (1)	0.230 (1)	−0.034 (1)	8 (1)
C(1)	0.162 (1)	0.163 (1)	0.203 (2)	5 (1)
C(11)	0.332 (2)	0.393 (1)	0.372 (1)	4 (1)
C(12)	0.133 (2)	0.424 (1)	0.324 (1)	5 (2)
C(13)	0.269 (2)	0.317 (1)	0.475 (2)	6 (2)
C(21)	0.044 (2)	0.297 (1)	0.240 (2)	6 (2)
C(22)	0.196 (2)	0.191 (2)	0.390 (2)	9 (3)
C(31)	0.174 (2)	0.193 (1)	0.042 (2)	5 (1)
C(32)	0.344 (2)	0.096 (1)	0.191 (2)	6 (2)
C(41)	0.387 (2)	0.342 (1)	0.173 (2)	5 (2)
C(42)	0.494 (2)	0.188 (1)	0.277 (2)	5 (2)
C(43)	0.329 (2)	0.242 (1)	0.046 (2)	6 (2)

Table VI. Positional Parameters and B(eq) Values for the Atoms in the Cluster Anion of $[Cp_2Co]$[**2b**]

atom	x	y	z	B(eq), Å^2
Bi(1)	0.4757 (1)	0.0104 (2)	0.6481 (1)	2.83 (7)
Co(1)	0.6366 (3)	0.0621 (5)	0.7139 (4)	2.8 (3)
Co(2)	0.5836 (4)	−0.1417 (5)	0.7347 (5)	3.4 (3)
O(11)	0.792 (2)	0.024 (3)	0.829 (2)	6 (1)
O(12)	0.704 (2)	0.050 (2)	0.534 (3)	5.6 (9)
O(13)	0.616 (3)	0.289 (4)	0.742 (3)	8 (1)
O(21)	0.710 (2)	−0.224 (3)	0.868 (2)	6 (1)
O(22)	0.674 (3)	−0.214 (3)	0.569 (3)	9 (1)
O(23)	$^1/_2$	−0.341 (5)	$^3/_4$	8 (2)
C(11)	0.734 (4)	0.035 (5)	0.785 (4)	7 (2)
C(12)	0.675 (2)	0.060 (4)	0.606 (3)	2.6 (9)
C(13)	0.623 (3)	0.190 (4)	0.731 (4)	5 (1)
C(21)	0.664 (3)	−0.192 (4)	0.816 (3)	4 (1)
C(22)	0.636 (4)	−0.176 (4)	0.636 (4)	5 (1)
C(23)	$^1/_2$	−0.249 (6)	$^3/_4$	4 (2)

Table VII. Intramolecular Distances (Å) within the Cluster Anion for [PPN][**2a**]

Sb(1)–Sb(2)	2.911 (1)	O(1)–C(1)	1.18 (2)
Sb(1)–Co(1)	2.611 (2)	O(11)–C(11)	1.17 (2)
Sb(1)–Co(2)	2.640 (2)	O(12)–C(12)	1.13 (2)
Sb(1)–Co(3)	2.685 (2)	O(13)–C(13)	1.13 (2)
Sb(1)–Co(4)	2.609 (2)	O(21)–C(21)	1.13 (2)
Sb(2)–Co(1)	2.605 (2)	O(22)–C(22)	1.16 (2)
Sb(2)–Co(2)	2.663 (2)	O(31)–C(31)	1.16 (2)
Sb(2)–Co(3)	2.692 (2)	O(32)–C(32)	1.15 (2)
Sb(2)–Co(4)	2.616 (3)	O(41)–C(41)	1.17 (2)
Co(1)–Co(2)	2.725 (3)	O(42)–C(42)	1.16 (2)
Co(2)–Co(3)	2.510 (3)	O(43)–C(43)	1.14 (2)
Co(3)–Co(4)	2.694 (3)	Co(1)–C(11)	1.75 (2)
Co(1)–C(12)	1.79 (2)	Co(1)–C(13)	1.81 (2)
Co(2)–C(1)	1.93 (1)	Co(2)–C(21)	1.80 (1)
Co(2)–C(22)	1.78 (2)	Co(3)–C(1)	1.86 (2)
Co(3)–C(31)	1.77 (2)	Co(3)–C(32)	1.77 (2)
Co(4)–C(41)	1.74 (2)	Co(4)–C(42)	1.77 (2)
Co(4)–C(43)	1.74 (2)		

Discussion

The reaction of $SbCl_3$ with $Na[Co(CO)_4]$ leads to an unstable, hexane-soluble compound **1a** with an infrared spectrum nearly identical with that of $Bi\{Co(CO)_4\}_3$ (**1b**), which we conclude to be $Sb\{Co(CO)_4\}_3$. Because of the instability of this complex, it was not possible to characterize it more completely. At first the

Table VIII. Intramolecular Bond Angles (deg) for the Cluster Anion in [PPN][**2a**]

Co(4)–Sb(1)–Co(1)	102.53 (7)	C(12)–Co(1)–Sb(2)	90.2 (6)
Co(4)–Sb(1)–Co(2)	104.87 (7)	C(12)–Co(1)–Sb(1)	153.4 (6)
Co(4)–Sb(1)–Co(3)	61.18 (7)	C(12)–Co(1)–Co(2)	97.2 (5)
Co(4)–Sb(1)–Sb(2)	56.26 (6)	C(13)–Co(1)–Sb(2)	149.6 (5)
Co(1)–Sb(1)–Co(2)	62.53 (7)	C(13)–Co(1)–Sb(1)	90.6 (5)
Co(1)–Sb(1)–Co(3)	105.69 (7)	C(13)–Co(1)–Co(2)	91.0 (5)
Co(1)–Sb(1)–Sb(2)	55.97 (5)	Sb(2)–Co(1)–Sb(1)	67.85 (6)
Co(2)–Sb(1)–Co(3)	56.24 (6)	Sb(2)–Co(1)–Co(2)	59.90 (6)
Co(2)–Sb(1)–Sb(2)	57.09 (5)	Sb(1)–Co(1)–Co(2)	59.25 (6)
Co(3)–Sb(1)–Sb(2)	57.34 (5)	C(22)–Co(2)–C(21)	100.0 (7)
Co(1)–Sb(2)–Co(4)	102.49 (7)	C(22)–Co(2)–C(1)	98.5 (7)
Co(1)–Sb(2)–Co(2)	62.30 (7)	C(22)–Co(2)–Co(3)	123.3 (6)
Co(1)–Sb(2)–Co(3)	105.67 (7)	C(22)–Co(2)–Sb(1)	92.7 (5)
Co(1)–Sb(2)–Sb(1)	56.18 (5)	C(22)–Co(2)–Sb(2)	153.8 (5)
Co(4)–Sb(2)–Co(2)	104.00 (7)	C(22)–Co(2)–Co(1)	98.2 (5)
Co(4)–Sb(2)–Co(3)	60.99 (6)	C(21)–Co(2)–C(1)	100.5 (6)
Co(4)–Sb(2)–Sb(1)	56.02 (5)	C(21)–Co(2)–Co(3)	126.1 (5)
Co(2)–Sb(2)–Co(3)	55.90 (6)	C(21)–Co(2)–Sb(1)	151.9 (5)
Co(2)–Sb(2)–Sb(1)	56.33 (5)	C(21)–Co(2)–Sb(2)	92.9 (5)
Co(3)–Sb(2)–Sb(1)	57.10 (5)	C(21)–Co(2)–Co(1)	95.0 (5)
C(11)–Co(1)–C(12)	103.0 (7)	C(1)–Co(2)–Co(3)	47.4 (5)
C(11)–Co(1)–C(13)	106.2 (7)	C(1)–Co(2)–Sb(1)	102.2 (5)
C(11)–Co(1)–Sb(2)	97.0 (6)	C(1)–Co(2)–Sb(2)	101.3 (4)
C(11)–Co(1)–Sb(1)	94.8 (6)	C(1)–Co(2)–Co(1)	154.8 (5)
C(11)–Co(1)–Co(2)	149.4 (6)	Co(3)–Co(2)–Sb(1)	62.78 (7)
C(12)–Co(1)–C(13)	103.0 (8)	Co(3)–Co(2)–Sb(2)	62.63 (7)
Co(3)–Co(2)–Co(1)	107.4 (1)	C(41)–Co(4)–C(42)	107.1 (8)
Sb(1)–Co(2)–Sb(2)	66.59 (5)	C(41)–Co(4)–Sb(1)	96.1 (6)
Sb(1)–Co(2)–Co(1)	58.22 (6)	C(41)–Co(4)–Sb(2)	102.7 (6)
Sb(2)–Co(2)–Co(1)	57.80 (6)	C(41)–Co(4)–Co(3)	154.8 (5)
C(31)–Co(3)–C(32)	96.8 (7)	C(43)–Co(4)–C(42)	105.1 (9)
C(31)–Co(3)–C(1)	97.0 (7)	C(43)–Co(4)–Sb(1)	89.9 (6)
C(31)–Co(3)–Co(2)	125.7 (6)	C(43)–Co(4)–Sb(2)	148.8 (6)
C(31)–Co(3)–Sb(1)	155.3 (5)	C(43)–Co(4)–Co(3)	89.6 (6)
C(31)–Co(3)–Sb(2)	95.7 (5)	C(42)–Co(4)–Sb(1)	149.1 (6)
C(31)–Co(3)–Co(4)	98.9 (5)	C(42)–Co(4)–Sb(2)	87.0 (6)
C(32)–Co(3)–C(1)	98.2 (7)	C942)–Co(4)–Co(3)	91.8 (6)
C(32)–Co(3)–Co(2)	125.4 (5)	Sb(1)–Co(4)–Sb(2)	67.72 (6)
C(32)–Co(3)–Sb(1)	95.3 (5)	Sb(1)–Co(4)–Co(3)	60.81 (7)
C(32)–Co(3)–Sb(2)	154.6 (5)	Sb(2)–Co(4)–Co(3)	60.89 (7)
C(32)–Co(3)–Co(4)	98.0 (5)	O(1)–C(1)–Co(3)	142 (1)
C(1)–Co(3)–Co(2)	49.7 (5)	O(1)–C(1)–Co(2)	135 (1)
C(1)–Co(3)–Sb(1)	102.5 (5)	Co(3)–C(1)–Co(2)	82.9 (6)
C(1)–Co(3)–Sb(2)	102.2 (5)	O(11)–C(11)–Co(1)	180 (2)
C(1)–Co(3)–Co(4)	155.7 (5)	O(12)–C(12)–Co(1)	176 (2)
Co(2)–Co(3)–Sb(1)	60.97 (7)	O(13)–C(13)–Co(1)	177 (1)
Co(2)–Co(3)–Sb(2)	61.47 (7)	O(21)–C(21)–Co(2)	178 (1)
Co(2)–Co(3)–Co(4)	106.1 (1)	O(22)–C(22)–Co(2)2	179 (1)
Sb(1)–Co(3)–Sb(2)	65.56 (5)	O(31)–C(31)–Co(3)	175 (1)
Sb(1)–Co(3)–Co(4)	58.01 (7)	O(32)–C(32)–Co(3)	177 (1)
Sb(2)–Co(3)–Co(4)	58.12 (7)	O(41)–C(41)–Co(4)	177 (2)
C(41)–Co(4)–C(43)	100.9 (9)	O(42)–C(42)–Co(4)	177 (1)
O(43)–C(43)–Co(4)	177 (2)		

Table IX. Intramolecular Distances (Å) within the Cluster Anion for [PPN][**2a**]

Sb(1)–Sb(2)	2.882 (2)	O(1)–C(1)	1.17 (3)
Sb(1)–Co(1)	2.656 (3)	O(11)–C(11)	1.15 (3)
Sb(1)–Co(2)	2.639 (4)	O(12)–C(12)	1.18 (2)
Sb(1)–Co(3)	2.622 (3)	O(13)–C(13)	1.15 (3)
Sb(1)–Co(4)	2.672 (3)	O(21)–C(21)	1.17 (3)
Sb(2)–Co(1)	2.632 (3)	O(22)–C(22)	1.16 (5)
Sb(2)–Co(2)	2.616 (4)	O(31)–C(31)	1.17 (3)
Sb(2)–Co(3)	2.625 (3)	O(32)–C(32)	1.17 (3)
Sb(2)–Co(4)	2.676 (4)	O(41)–C(41)	1.15 (4)
Co(1)–Co(2)	2.716 (5)	O(42)–C(42)	1.14 (3)
Co(2)–Co(3)	2.646 (5)	O(43)–C(43)	1.16 (3)
Co(3)–Co(4)	2.717 (5)	Co(1)–C(11)	1.76 (3)
Co(1)–C(12)	1.72 (2)	Co(1)–C(13)	1.77 (3)
Co(2)–C(1)	1.94 (2)	Co(2)–C(21)	1.71 (2)
Co(2)–C(22)	1.75 (4)	Co(3)–C(1)	1.87 (3)
Co(3)–C(31)	1.70 (2)	Co(3)–C(32)	1.74 (2)
Co(4)–C(41)	1.77 (3)	Co(4)–C(42)	1.76 (2)
Co(4)–C(43)	1.74 (2)		

Table X. Intramolecular Bond Angles (deg) within the Cluster Anion of [PPN][**2a**]

Co(2)-Sb(1)-Co(3)	60.4 (1)	C(11)-Co(1)-Sb(2)	94.0 (7)
Co(2)-Sb(1)-Co(1)	61.7 (1)	C(11)-Co(1)-Sb(1)	98.9 (7)
Co(2)-Sb(1)-Co(4)	107.9 (1)	C(11)-Co(1)-Co(2)	149.1 (8)
Co(2)-Sb(1)-Sb(2)	56.53 (7)	C(13)-Co(1)-Sb(2)	91.9 (7)
Co(3)-Sb(1)-Co(1)	107.6 (1)	C(13)-Co(1)-Sb(1)	146.8 (8)
Co(3)-Sb(1)-Co(4)	61.8 (1)	C(13)-Co(1)-Co(2)	88.8 (8)
Co(3)-Sb(1)-Sb(2)	56.74 (7)	Sb(1)-Co(1)-Sb(2)	66.05 (8)
Co(1)-Sb(1)-Co(4)	101.4 (1)	Sb(2)-Co(1)-Co(2)	58.5 (1)
Co(1)-Sb(1)-Sb(2)	56.58 (7)	Sb(1)-Co(1)-Co(2)	58.8 (1)
Co(4)-Sb(1)-Sb(2)	57.47 (8)	C(21)-Co(2)-C(22)	108 (1)
Co(3)-Sb(2)-Co(2)	60.7 (1)	C(21)-Co(2)-C(1)	100 (1)
Co(3)-Sb(2)-Co(1)	108.25 (9)	C(21)-Co(2)-Sb(2)	153 (1)
Co(3)-Sb(2)-Co(4)	61.7 (1)	C(21)-Co(2)-Sb(1)	90 (1)
Co(3)-Sb(2)-Sb(1)	56.63 (7)	C(21)-Co(2)-Co(3)	119.7 (9)
Co(2)-Sb(2)-Co(1)	62.3 (1)	C(21)-Co(2)-Co(1)	98.8 (9)
Co(2)-Sb(2)-Co(4)	108.4 (1)	C(22)-Co(2)-C(1)	95 (1)
Co(2)-Sb(2)-Sb(1)	57.13 (9)	C(22)-Co(2)-Sb(2)	92 (1)
Co(1)-Sb(2)-Co(4)	101.9 (1)	C(22)-Co(2)-Sb(1)	157 (1)
Co(1)-Sb(2)-Sb(1)	57.37 (7)	C(22)-Co(2)-Co(3)	120 (1)
Co(4)-Sb(2)-Sb(1)	57.32 (7)	C(22)-Co(2)-Co(1)	102 (1)
C(12)-Co(1)-C(11)	104 (1)	C(1)-Co(2)-Sb(2)	95.6 (7)
C(12)-Co(1)-C(13)	104 (1)	C(1)-Co(2)-Sb(1)	97.2 (8)
C(12)-Co(1)-Sb(2)	150.5 (8)	C(1)-Co(2)-Co(3)	44.9 (8)
C(12)-Co(1)-Sb(1)	87.9 (7)	C(1)-Co(2)-Co(1)	150.0 (8)
C(12)-Co(1)-Co(2)	97 (1)	Sb(1)-Co(2)-Sb(2)	66.5 (1)
C(11)-Co(1)-C(13)	108 (1)	Sb(2)-Co(2)-Co(3)	59.9 (1)
Sb(2)-Co(2)-Co(1)	59.1 (1)	C(43)-Co(4)-C(41)	104 (1)
Sb(1)-Co(2)-Co(3)	59.5 (1)	C(43)-Co(4)-Sb(1)	97 (1)
Sb(1)-Co(2)-Co(1)	59.4 (1)	C(43)-Co(4)-Sb(2)	139 (1)
Co(3)-Co(2)-Co(1)	105.2 (2)	C(43)-Co(4)-Co(3)	81 (1)
C(31)-Co(3)-C(32)	109 (1)	C(42)-Co(4)-C(41)	107 (1)
C(31)-Co(3)-C(1)	94 (1)	C(42)-Co(4)-Sb(1)	147 (1)
C(31)-Co(3)-Sb(1)	92.4 (7)	C(42)-Co(4)-Sb(2)	82 (1)
C(31)-Co(3)-Sb(2)	157.5 (8)	C(42)-Co(4)-Co(3)	104 (1)
C(31)-Co(3)-Co(2)	118.1 (8)	C(41)-Co(4)-Sb(1)	87.2 (8)
C(31)-Co(3)-Co(4)	103 (1)	C(41)-Co(4)-Sb(2)	110.9 (9)
C(32)-Co(3)-C(1)	100 (1)	C(41)-Co(4)-Co(3)	145.4 (8)
C(32)-Co(3)-Sb(1)	150 (1)	Sb(2)-Co(4)-Sb(1)	65.2 (1)
C(32)-Co(3)-Sb(2)	88.0 (9)	Sb(1)-Co(4)-Co(3)	58.2 (1)
C(32)-Co(3)-Co(2)	122 (1)	Sb(2)-Co(4)-Co(3)	58.2 (1)
C(32)-Co(3)-Co(4)	94 (1)	O(11)-C(11)-Co(1)	175 (2)
C(1)-Co(3)-Sb(1)	99.7 (7)	O(12)-C(12)-Co(1)	177 (2)
C(1)-Co(3)-Sb(2)	97.1 (6)	O(13)-C(13)-Co(1)	175 (2)
C(1)-Co(3)-Co(2)	47.1 (7)	O(21)-C(21)-Co(2)	174 (2)
C(1)-Co(3)-Co(4)	153.3 (7)	O(22)-C(22)-Co(2)	178 (3)
Sb(2)-Co(3)-Sb(1)	66.63 (8)	O(1)-C(1)-Co(3)	140 (2)
Sb(1)-Co(3)-Co(2)	60.1 (1)	O(1)-C(1)-Co(2)	132 (2)
Sb(1)-Co(3)-Co(4)	60.0 (1)	Co(3)-C(1)-Co(2)	88 (1)
Sb(2)-Co(3)-Co(2)	59.5 (1)	O(31)-C(31)-Co(3)	178 (3)
Sb(2)-Co(3)-Co(4)	60.1 (1)	O(32)-C(32)-Co(3)	175 (3)
Co(2)-Co(3)-Co(4)	106.3 (1)	O(41)-C(41)-Co(4)	175 (3)
C(43)-Co(4)-C(42)	107 (1)	O(42)-C(42)-Co(4)	176 (3)
O(43)-C(43)-Co(4)	171 (3)		

Table XI. Bond Distances (Å) within the Cluster Anion in [Cp_2Co][**2b**]

Bi(1)-Bi(1A)	3.078 (3)	Bi(1)-Co(1)	2.677 (5)
Bi(1)-Co(1A)	2.712 (6)	Bi(1)-Co(2)	2.730 (7)
Bi(1)-Co(2A)	2.817 (7)	Co(1)-Co(2)	2.716 (9)
Co(2)-Co(2A)	2.54 (1)	Co(2)-C(23)	1.86 (5)
Co(1)-C(13)	1.65 (5)	Co(1)-C(12)	1.69 (5)
Co(1)-C(11)	1.82 (6)	Co(2)-C(22)	1.70 (6)
Co(2)-C(21)	1.81 (5)	C(11)-O(11)	1.10 (6)
C(12)-O(12)	1.15 (5)	C(13)-O(13)	1.27 (6)
C(21)-O(21)	1.11 (5)	C(22)-O(22)	1.24 (6)
C(23)-O(23)	1.16 (8)		

instability was conjectured to arise from CO loss, as **1b** readily loses CO to produce **3**. No compound corresponding to $SbCo_3(CO)_9$ has been observed, and the products found here suggest that complicated disproportionation reactions are taking place instead.

The inability to form the $[Sb\{Co(CO)_4\}_4]^-$ anion may be attributed to the lower Lewis acidity of Sb as compared to Bi. On the other hand, it is interesting to note that the electron-precise cation $[Sb\{Co(CO)_3(PPh_3)\}_4]^+$ [22] has been reported and structurally

Table XII. Bond Angles (deg) within the Cluster Anion in [Cp_2Co][**2b**]

Co(1)-Bi(1)-Co(2)	59.2 (2)	Co(1)-Bi(1)-Co(1)A	103.3 (2)
Co(1)-Bi(1)-Co(2A)	103.8 (2)	Co(1)-Bi(1)-Bi(1A)	55.7 (1)
Co(1)-Bi(1A)-Co(2)	59.9 (2)	Co(1)-Bi(1A)-Co(2A)	100.6 (2)
Co(1)-Bi(1A)-Bi(1)	54.7 (1)	Co(2)-Bi(1)-Co(2A)	54.6 (2)
Co(2)-Bi(1)-Bi(1A)	57.7 (1)	Co(2)-Bi(1A)-Bi(1)	55.5 (1)
C(13)-Co(1)-C(12)	102 (3)	C(13)-Co(1)-C(11)	101 (3)
C(13)-Co(1)-Bi(1)	100 (2)	C(13)-Co(1)-Bi(1A)	93 (2)
C(13)-Co(1)-Co(2)	151 (2)	C(12)-Co(1)-C(11)	105 (2)
C(12)-Co(1)-Bi(1)	88 (1)	C(12)-Co(1)-Bi(1A)	155 (1)
C(12)-Co(1)-Co(2)	101 (2)	C(11)-Co(2)-Bi(1)	152 (2)
C(11)-Co(1)-Bi(1A)	91 (2)	C(11)-Co(1)-Co(2)	89 (2)
Bi(1)-Co(1)-Bi(1A)	69.6 (1)	Bi(1)-Co(1)-Co(2)	63.0 (2)
Bi(1)-Co(1A)-Co(2A)	60.4 (2)	C(22)-Co(2)-C(21)	99 (2)
C(22)-Co(2)-C(23)	103 (2)	C(22)-Co(2)-Co(2A)	127 (2)
C(22)-Co(2)-Co(1)	91 (2)	C(22)-Co(2)-Bi(1A)	150 (2)
C(22)-Co(2)-Bi(1)	93 (2)	C(21)-C(2)-C(23)	97 (2)
C(21)-Co(2)-Co(2A)	123 (2)	C(21)-Co(2)-C(1)	102 (2)
C(21)-Co(2)-Bi(1A)	93 (1)	C(21)-C(2)-Bi(1)	157 (2)
C(23)-Co(2)-Co(2A)	47 (2)	C(23)-Co(2)-C(1)	155 (2)
C(23)-Co(2)-Bi(1A)	103 (1)	C(23)-Co(2)-Bi(1)	100 (1)
Co(1)-Co(2)-Co(2A)	107.9 (2)	Co(1)-Co(2)-Bi(1A)	59.7 (2)
Co(1)-Co(2)-Bi(1)	57.8 (2)	Bi(1)-Co(2)-Bi(1A)	67.4 (2)
Co(1)-C(11)-O(11)	176 (6)	Co(1)-C(12)-O(12)	175 (4)
Co(1)-C(13)-O(13)	177 (5)	Co(2)-C(21)-O(21)	176 (5)
Co(2)-C(22)-O(22)	172 (5)	Co(2)-C(23)-O(23)	137 (2)
Co(2)-C(23)-Co(2A)	86 (3)		

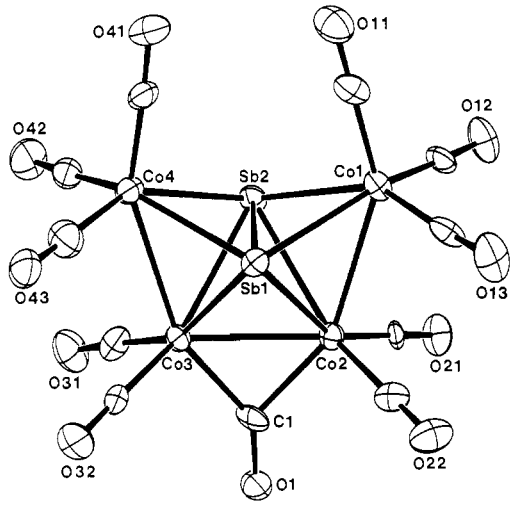

Figure 1. ORTEP drawing of $[\mathbf{2a}]^{2-}$, showing 50% anisotropic displacement parameters.

characterized. Attempts to produce the corresponding unsubstituted compound by reaction of $[Co(CO)_4]^-$ with $SbCl_5$ were not successful and instead led rather cleanly to $[\mathbf{2a}]^-$.

The chemistry of the bismuth system has proven to be somewhat different from that for antimony. Compound **1b** is unstable in solution as is **1a**, but the product is not that of complex redox reactions but rather of simple CO loss to give **3**. Reduction of **3** with either sodium naphthalenide or cobaltocene promotes a complicated rearrangement producing $[\mathbf{2b}]^-$. No $[\mathbf{2b}]^{2-}$ has been observed in those reactions.

A chemically and electrochemically reversible 1e redox cycle relates the $[\mathbf{2}]^{-/2-}$ couples. Very little structural change occurs during this cycle in the case of $[\mathbf{2a}]^{-/2-}$ except for the lengthening of the CO-bridged Co–Co bond; vide infra. The paramagnetic monoanions are qualitatively more stable than their corresponding dianions.

The structures of $[\mathbf{2a}]^-$ and $[\mathbf{2b}]^-$ are qualitatively very similar to that of $[\mathbf{2a}]^{2-}$ (Figure 1). The structures of these anions are also qualitatively the same as that previously reported for $Os_6(CO)_{18}$,[19] $Os_4H_2(CO)_{12}(AuPPh_3)_2$,[23] and $Ni_3Os_3(CO)_9(Cp)_3$.[24]

(22) (a) Cullen, W. R.; Patmore, D. J.; Sams, J. R. *Inorg. Chem.* **1973**, *12*, 867. (b) Cobbledick, R. E.; Einstein, F. W. B. *Acta Crystallogr., Sect. B* **1979**, *B35*, 2041.

(23) Johnson, B. F. G.; Kaner, D. A.; Lewis, J.; Raithby, P.; Taylor, M. J. *Polyhedron* **1982**, *1*, 105.

The $[Me_4N]^+$ salt of $[\mathbf{2b}]^-$ reported by Martinengo and Ciani is essentially the same as that observed here for the $[Cp_2Co]^+$ salt. The Sb–Sb distances are 2.911 (1) Å in $[\mathbf{2a}]^-$ and 2.882 (2) Å in $[\mathbf{2a}]^{2-}$. These values are similar to the longest Sb–Sb distances in the Zintl ion, Sb_7^{3-} [range: 2.693 (4)–2.880 (4) Å],[25] slightly long compared to the Sb–Sb single-bond distance of 2.837 (1) Å in Ph_4Sb_2,[26] and much longer than the Sb–Sb distances of 2.663 Å in $Sb_2\{W(CO)_5\}_3$[27] and 2.678 (1) Å in $Cp_2Mo_2(CO)_4Sb_2$,[28] which are considered to exhibit some degree of multiple Sb–Sb bond character. The Sb–Co(av) distances of 2.640 (36) Å in $[\mathbf{2a}]^-$ and 2.642 (23) Å in $[\mathbf{2a}]^{2-}$ are longer than the Sb–Co distances in $[Sb\{Co(CO)_3PPh_3\}_4]^+$[22] and the cubane $Sb_4Co_4(CO)_{12}$[29] [2.596 and 2.614 (2) Å, respectively], which are the only other known Sb/Co compounds. As in $[\mathbf{2b}]^-$, the Co–Co distances in $[\mathbf{2a}]^{-/2-}$ bridged by the carbonyl ligand are significantly shorter than the other Co–Co distances ($[\mathbf{2a}]^-$, 2.510 (3) Å vs 2.725 (3) and 2.694 (3) Å; $[\mathbf{2a}]^{2-}$, 2.646 (5) Å vs 2.716 (5) and 2.717 (5) Å).

In the comparison of the structures of $[\mathbf{2a}]^-$ and $[\mathbf{2a}]^{2-}$, the most significant structural change upon reduction is the 0.136-Å increase in the Co(2)–Co(3) distance ($[\mathbf{2a}]^-$, 2.510 (3) Å; $[\mathbf{2a}]^{2-}$, 2.646 (5) Å). This change causes the dihedral angle between the Sb(1)–Sb(2)–Co(2) plane and the Sb(1)–Sb(2)–Co(3) plane to increase from 68.2 to 74.1° and the Co(2)–C(1)–Co(3) angle to increase from 82.9 (6) to 88 (1)°. The other distances show much smaller differences; i.e., Sb–Sb and Sb–Co(2,3) decrease slightly overall, while Sb–Co(1,4) increase a small amount as other framework distances remain statistically identical, including those of the bridging carbonyl ligand. Thus, it is plausible that the HOMO in $[\mathbf{2a}]^{-/2-}$ is an antibonding orbital primarily localized on the CO-bridged Co–Co bond. This is consistent with MO calculations; vide infra.

Similar comparisons can be made in the bismuth system. Since the ORTEP diagram of $[\mathbf{2b}]^-$ is not presented due to its similarity to $[\mathbf{2a}]^-$, a difference in numbering schemes should be noted. Here the molecule lies upon a 2-fold axis, and there are only one unique bismuth and two unique cobalt atoms. The capping cobalt atom is Co(1) and the cobalt atom attached to the bridging carbonyl is Co(2), consistent with the numbering in $[\mathbf{2a}]^{-/2-}$. The symmetry equivalents are Co(1a) and Co(2a), respectively. As expected, the Bi–Co(av) bond length in $[\mathbf{2b}]^-$ is longer than the Sb–Co(av) distances in both of the antimony anions, and the unbridged Co–Co bond lengths are all statistically similar. Also, the length of the Co–Co bond bridged by the carbonyl ligand in $[\mathbf{2b}]^-$ is statistically similar to that of $[\mathbf{2a}]^-$.

The Bi–Bi distance in the bismuth anion is 3.078 (3) Å and lies in the range seen for other Bi–Bi single bonds: $[Bi_4Fe_4(CO)_{13}]^{2-}$ (3.157 Å),[30] $[Bi_2Fe_2Co(CO)_{10}]^-$ (3.092 (2) Å),[31] Bi_2Ph_4 (2.990 (2) Å),[32] $Bi_2(SiMe_3)_4$ (3.035 (3) Å),[33] $Bi_2Os_4(CO)_{12}$ (3.017 (2) Å),[34] and Bi_9^{5+} (3.08 Å).[35] The distances observed in $MeBiW(CO)_5\{W_2(CO)_8Bi_2\}$ (2.796 (1) Å),[36] Bi_4^{2-} [2.936 (2) and 2.941 (2) Å],[37] and $Bi_2W_3(CO)_{15}$ (2.818 (3) Å)[38] are shorter and are believed to result from multiple Bi–Bi bonding. The average Bi–Co bond length in $[Cp_2Co][\mathbf{2b}]$ is 2.734 Å, as compared to 2.766 Å in $Bi\{Co(CO)_4\}_3$,[11] 2.624 (3) Å in $BiCo_3(CO)_9$,[12] 2.906 (1) Å in $[Cp_2Co][Bi\{Co(CO)_4\}_4]$,[20] and 2.746 Å in $Bi_4Co_4(CO)_{12}$.[39] The distance between the capping cobalt and the cobalt in the M_2E_2 tetrahedron (2.716 (9) Å) is longer than the CO-bridged Co–Co bond. The Co–Co distances in $BiCo_3(CO)_9$ and $Co_2(CO)_8$[40] are 2.548 (6) and 2.524 (2) Å, respectively, thus showing the CO-bridged bond length to be similar to these values and that between Co(1) and Co(2) to be significantly longer.

Both $[\mathbf{2a}]^-$ and $[\mathbf{2b}]^-$ are paramagnetic and contain 17 skeletal electrons, or five more electrons than required for a normal bicapped tetrahedron or monocapped trigonal bipyramid. Each show an ESR signal indicative of one unpaired electron although the signals were broad and no fine structure was resolved under the conditions employed. $[\mathbf{2a}]^{2-}$ possesses 18 skeletal electrons and is thus even more "electron rich". An electron-precise tetrahedron, i.e. $[Sb_2Co_2(CO)_4(\mu\text{-}CO)]^{2-}$, possesses 12 skeletal electrons. In the normal situation each capping unit supplies no additional skeletal electrons to the cluster.[1-5] Teo, however, has allowed for the possibility of 4 extra skeletal electrons.[4] In the present case there are in fact 5 additional electrons for $[\mathbf{2a}]^-$ and $[\mathbf{2b}]^-$ and 6 in $[\mathbf{2a}]^{2-}$!

Alternatively, these clusters may be derived from a nido pentagonal bipyramid (**4**; 16 skeletal electrons predicted) or an arachno dodecahedron (**5**; 18 skeletal electrons predicted). A similar ambiguity exists in the description of the geometry for the seven-vertex $Cp_2Mo_2Co_2E_3$ (E = S, Te),[41] whose description lies between a bicapped trigonal bipyramid and pentagonal bipyramid. Even though the dianions $[\mathbf{2}]^{2-}$ have an 18-electron count, the arachno dodecahedral view presupposes *no* E–E bonding, which is apparently present. There is a difference between views **4** and **5** in the predicted apical–apical atom separations. For the nido pentagonal bipyramid this separation is only 1.05 times that of the edge distance whereas in a D_{2d} arachno dodecahedron the corresponding distance is 1.29 times the edge length. Thus **4** is a better model than **5** and these molecules do not conform to conventional electron-counting formalisms. This is supported by MO calculations at the extended Hückel level, which were used to establish the bonding here as well as in other electron-rich M_4E_2 systems. We shall present these results by developing the molecular orbitals from the pentagonal bipyramidal, **4**, and the bicapped tetrahedral, **2**, viewpoints.

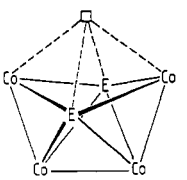

4

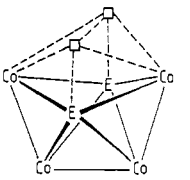

5

Derivation of the Nido Pentagonal Bipyramid. In the derivation of the nido pentagonal bipyramid, N-vertex closo and nido clusters are structurally related by the fact that the latter can be seen as the result of a bond opening in the former. For example, the breaking of a metal–metal bond in an M_4E_2 octahedron gives a nido pentagonal bipyramid, as shown in **4**. This leads to the stabilization of one antibonding orbital in the octahedron, which becomes nonbonding in the pentagonal bipyramid. The stabilization of the MO, localized on the broken bond, allows the open nido form to possess two more electrons than its related closo cluster. Some of us have previously reported extended Hückel calculations on closo- and nido-type M_4E_2 clusters and related

(24) Sappa, E.; Lanfranchi, M.; Tiripicchio, A.; Camellini, M. T. *J. Chem. Soc., Chem. Commun.* **1981**, 995.
(25) Adolphson, D. G.; Corbett, J. D.; Merryman, D. J. *J. Am. Chem. Soc.* **1976**, *98*, 7234.
(26) Van Deuter, K.; Rehder, D. *Cryst. Struct. Commun.* **1980**, *9*, 167.
(27) Huttner, G.; Weber, U.; Sigwarth, B.; Scheidsteger, O. *Angew. Chem., Int. Ed. Engl.* **1982**, *21*, 215.
(28) Harper, J. R.; Rheingold, A. L. *J. Organomet. Chem.* **1990**, *390*, C36.
(29) Faust, A. S.; Dahl, L. F. *J. Am. Chem. Soc.* **1970**, *92*, 7337.
(30) Whitmire, K. H.; Albright, T. A.; Kang, S.-K.; Churchill, M. R.; Fettinger, J. C. *Inorg. Chem.* **1986**, *25*, 2799.
(31) Whitmire, K. H.; Raghuveer, K. S.; Churchill, M. R.; Fettinger, J. C.; See, R. F. *J. Am. Chem. Soc.* **1986**, *108*, 2778.
(32) Calderazzo, F.; Morrillo, A.; Pelizzi, G.; Poli, R. *J. Chem. Soc., Chem. Commun.* **1983**, 507.
(33) Mundt, O.; Becker, G.; Roessler, M.; Witthauer, C. *Z. Anorg. Allg. Chem.* **1983**, *506*, 42.
(34) Ang, H. G.; Hay, C. M.; Johnson, B. F. G.; Lewis, J.; Raithby, P. R.; Whitton, A. J. *J. Organomet. Chem.* **1987**, *330*, C5.
(35) Corbett, J. D. *Prog. Inorg. Chem.* **1976**, *21*, 129.
(36) Arif, A. M.; Cowley, A. H.; Norman, N. C.; Pakulski, M. *J. Am. Chem. Soc.* **1985**, *107*, 1062; *Inorg. Chem.* **1986**, *25*, 4836.
(37) Cisar, A.; Corbett, J. D. *Inorg. Chem.* **1977**, *16*, 2482.
(38) Huttner, G.; Weber, U.; Zsolnai, L. *Z. Naturforsch.* **1982**, *37B*, 707.
(39) (a) Johnson, R. E. Ph.D. Thesis, University of Wisconsin, 1981. (b) Ciani, G.; Moret, M.; Fumagalli, A.; Martinengo, S. *J. Organomet. Chem.* **1989**, *362*, 291.
(40) Sumner, G. G.; Klug, H. P.; Alexander, L. E. *Acta Crystallogr.* **1964**, *17*, 732.
(41) (a) Curtis, M. D.; Williams, P. D. *Inorg. Chem.* **1983**, *22*, 2662. (b) Rheingold, A. L. *Acta Crystallogr., Sect. C* **1987**, *C43*, 585.

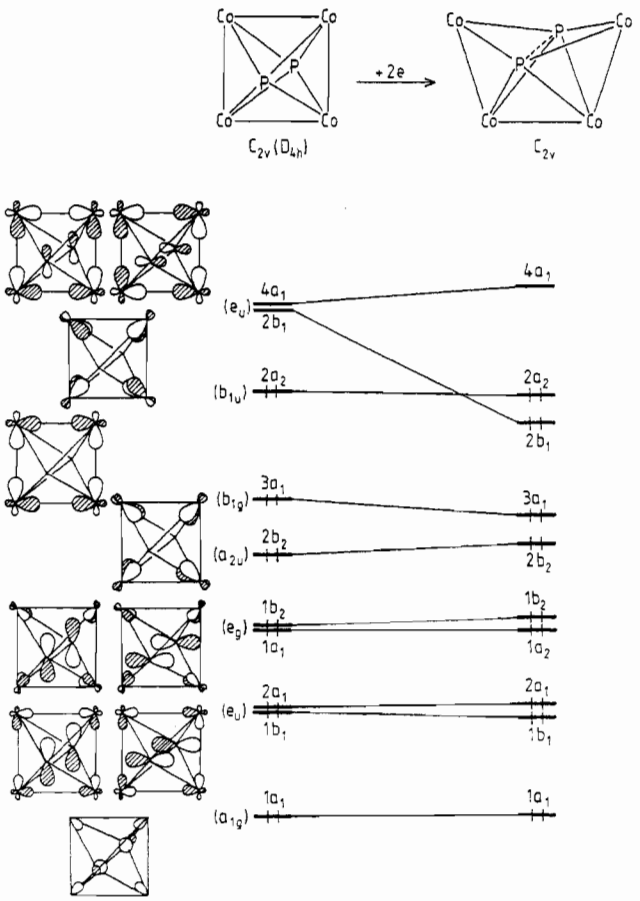

Figure 2. Skeletal molecular orbitals for closo (left-hand side) and nido (right-hand side) $Co_4(CO)_{12}(\mu_4\text{-}PH)_2$ models.

compounds,[42] and for the sake of understanding, we shall briefly summarize these previous results before addressing the analysis of $[\mathbf{2a}]^-$ and $[\mathbf{2a}]^{2-}$.

The regular electron count for a closo octahedral cluster is 14 skeletal electrons, and indeed, this is generally observed in E_6 main-group and M_6 organometallic compounds for which a significant HOMO–LUMO gap is calculated.[42,43] This gap, however, is much less important in M_6 clusters.[44] The reason lies in the energy of the t_{2g}* LUMO set, which is lower in the organometallic case. One component of this triply degenerate level is sketched in **6a** for the E_6 and in **6b** for the M_6 octahedra.

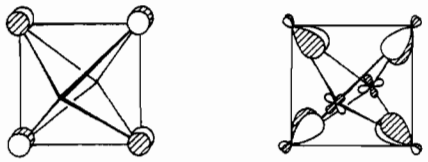

6a **6b**

Note that the two other components of **6** are identical but localized on the two other squares that circle the octahedron. These orbitals are the totally antibonding combinations of π frontier orbitals of the E or M groups. **6a** is strongly π antibonding. The antibonding character of **6b** is significantly weaker, being intermediate between π and δ types. Some destabilization of **6b**, however, is provided by mixing with low-lying "t_{2g}-type" orbitals of δ symmetry localized on the two apical M atoms that cap the square.[42-44] This destabilizing effect disappears when the two capping metallic units are replaced by main-group fragments from the third to sixth period. The result is depicted on the left-hand side of Figure 2, which shows the MO diagram of the closo-octahedral $[Co_4(CO)_{12}(\mu_4\text{-}PH)_2]^{2+}$ model of C_{2v} symmetry (D_{4h} pseudosymmetry). The weakly metal–metal antibonding $2a_2$ orbital, corresponding to **6b**, now lies in the middle of a large energy gap, a situation favoring the possibility of two electron counts: 14 skeletal electrons ($2a_2$ empty, the regular electron count) or 16 electrons ($2a_2$ occupied), depending upon the metal electronegativity. The opening of a Co–Co bond brings about the stabilization of a level of b_1 symmetry, as illustrated on the right-hand side of Figure 2, where the MO diagram of model $[Co_4(CO)_{12}(\mu_4\text{-}PH)_2]$ (**7**), having a nido C_{2v} open structure, has

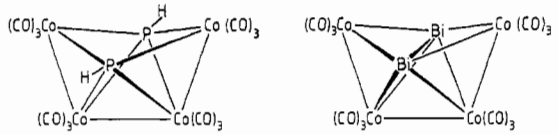

7 **8**

been represented. However, this level does not go down very deeply in energy, suggesting a unique possible electron count of 18 skeletal electrons. In fact, the geometry of **7** has been modeled on the experimental structure of the only structurally characterized cluster in this nido-type category, namely $Co_4(CO)_3[(F_2P)_2NMe]_4(\mu_4\text{-}PPh)_2$,[45] which possesses 18 skeletal electrons in agreement with our calculations.

A striking feature of this nido compound[45] and of most of the M_4E_2 closo-octahedral clusters in which the E groups occupy apical positions[42,46] is that the E···E separation lies in a range only $\approx$ 15–25% larger than the one corresponding to a single E–E bond. Indeed, in $Co_4(CO)_3[(F_2P)_2NMe]_4(\mu_4\text{-}PPh)_2$ the P···P separation is 2.44 Å.[45] This peculiarity can be partially considered as a size effect. Given M–M and M–E bond distances imposed by the major bonding interactions that are tangential to the cluster envelope, the resulting "nonbonding" E···E separation is necessarily rather short, at least when E is from the third or fourth period. In other words the octahedron or pentagonal bipyramid is contracted along the E···E axis. However, such a short nonbonding contact could not occur if the E···E interaction was not at least slightly attractive, and indeed it is significantly attractive, as shown by our calculations.[42] This is due to the $\sigma_{E\cdots E}$* frontier orbital lying at sufficiently high energy to avoid being significantly populated in the cluster, leading to a substantial positive E···E overlap population. So, both size and electronic factors contribute to the existence of short E···E contacts in *closo*- and *nido*-M_4E_2 clusters.

The orbital structure for **7** is very similar to that obtained for **8** as a model for $[\mathbf{2b}]^-$ or $[\mathbf{2a}]^-$ and $[\mathbf{2a}]^{2-}$. All compounds provide

(42) (a) Halet, J.-F.; Hoffmann, R.; Saillard, J.-Y. *Inorg. Chem.* **1985**, *25*, 1695. (b) Halet, J.-F.; Saillard, J.-Y. *New J. Chem.* **1987**, *11*, 315.
(43) Mingos, D. M. P. *J. Chem. Soc., Dalton Trans.* **1974**, 133.
(44) Note that, with a rather electronegative metal, the t_{2g}* set is rather low in energy and can be populated as in Ni_6Cp_6 (Paquette, M. S.; Dahl, L. F. *J. Am. Chem. Soc.* **1980**, *102*, 6621).
(45) Richmond, M. G.; Korp, J. D.; Kochi, J. K. *J. Chem. Soc., Chem. Commun.* **1985**, 1102.
(46) (a) Ryan, R. C.; Dahl, L. F. *J. Am. Chem. Soc.* **1975**, *97*, 6904. (b) Ryan, R. C.; Pittmann, C. U.; O'Connor, J. P.; Dahl, L. F. *J. Organomet. Chem.* **1980**, *193*, 247. (c) Wei, C. H.; Dahl, L. F. *Cryst. Struct. Commun.* **1975**, *4*, 583. (d) Lower, L. D.; Dahl, L. F. *J. Am. Chem. Soc.* **1976**, *98*, 5046. (e) Vahrenkamp, H.; Wucherer, E. J. *Angew. Chem., Int. Ed. Engl.* **1981**, *20*, 680. (f) Vahrenkamp, H.; Wucherer, E. J.; Wolters, D. *Chem. Ber.* **1983**, *116*, 1219. (g) Vahrenkamp, H.; Wolters, D. *Organometallics* **1982**, *1*, 874. (h) Jaeger, T.; Aime, S.; Vahrenkamp, H. *Organometallics* **1986**, *5*, 245. (i) Foster, S. P.; Mackay, K. M.; Nicholson, B. K. *J. Chem. Soc., Chem. Commun.* **1982**, 1156. (j) Vahrenkamp, H.; Wolters, D. *J. Organomet. Chem.* **1982**, *244*, C17. (k) Vahrenkamp, H.; Müller, M. *Chem. Ber.* **1983**, *116*, 2765. (l) Gusbeth, P.; Vahrenkamp, H. *Chem. Ber.* **1985**, *118*, 1746. (m) Arif, A. M.; Cowley, A. H.; Pakulski, M.; Hursthouse, M. B. Karauloz, A. *Organometallics* **1985**, *4*, 2227. (n) Foster, S. P.; Mackay, K. M.; Nicholson, B. K. *Inorg. Chem.* **1985**, *24*, 909. (o) Richmond, M. G.; Kochi, J. K. *Inorg. Chem.* **1986**, *25*, 1334. (p) Ohst, H. H.; Kochi, J. K. *Organometallics* **1986**, *5*, 1359. (q) Richmond, M. G.; Kochi, J. K. *Organometallics* **1987**, *6*, 254. (r) Van Tiel, M.; Mackay, K. M.; Nicholson, B. K. *J. Organomet. Chem.* **1987**, *326*, C101. (s) Mathur, P.; Thimmappa, B. H. S. *J. Organomet. Chem.* **1989**, *365*, 363. (t) A 20 skeletal electron octahedral M_4E_2 compound has been reported by: Fenske, D.; Hollnagel, A.; Merzweiler, K. *Angew. Chem., Int. Ed. Engl.* **1988**, *27*, 965. Calculations on this cluster are in progress.

a significant HOMO–LUMO gap for a count of 18 skeletal electrons. In **7**, as well as the other molecules the two extra electrons (in terms of the Wade–Mingos rules[1-3]) lie in the $2a_2$ level, which is derived from the π^* orbital, **6b**, in the M_4E_2 octahedron (see Figure 2). The distinguishing feature of **7** is that the two highest occupied orbitals, $2a_2$ and $2b_1$ in Figure 2, lie at a higher energy than the other occupied MO's, whereas, in the other molecules we have studied, this energy difference is smaller. Part of this is due to the fact that the geometry of the known molecule $Co_4(CO)_3[(F_2P)NMe]_4(\mu_4\text{-}PPh)_2$ is somewhat constrained due to the presence of the bidentate ligands. The Co–Co–Co angle (101°, average) is not fully relaxed to the ideal value for a nido pentagonal bipyramid (108°). This geometric constraint in turn allows for greater Co–Co antibonding in $2a_2$ and $2b_1$. It should also be noted, however, that allowing the Co–Co–Co angles to reach the ideal 108° value without varying the Co–Co or Co–P distances would result in an unrealistically short P···P distance of ~1.8 Å, which corresponds to a triple bond.

In all of the molecules that we have studied the E···E interaction is significant. One way to measure this is by the E···E overlap population, which was 0.483, 0.526, 0.395, and 0.416 for $[\mathbf{2a}]^-$, $[\mathbf{2a}]^{2-}$, **7**, and **8**, respectively. For reference, the Sb–Sb overlap population was computed to be 0.686 in H_4Sb_2 where the geometry was taken from Ph_4Sb_2.[26] Another measure that can be applied is the occupation of the E–E σ^* orbital, **9**. In H_4Sb_2 or another

9

molecule where an E–E single bond exists the σ^* occupation of an E_2 fragment will be close to zero. On the other hand, in a molecule where E···E interaction does not exist, the occupation of σ^* will be close to 2 electrons. For the cobalt clusters studied here it was computed to be 0.30, 0.27, 0.57, and 0.27 for $[\mathbf{2a}]^-$, $[\mathbf{2a}]^{2-}$, **7**, and **8**, respectively.

Derivation of the Bicapped Tetrahedron. In the bicapped tetrahedron derivation, the favored electron count for a $[Co_2E_2(CO)_{11}(\mu\text{-}CO)]^{2-}$ tetrahedron[47] is 12 skeletal electrons, and in fact, this unit is isolobal[2c,48] to tetrahedrane. Therefore, the nonconformity of $[\mathbf{2a}]^-$ and $[\mathbf{2a}]^{2-}$ with the Wade–Mingos rules must originate from a violation of the capping principle.[3c] In order to fully explore the genesis of this violation, we will first analyze a simple main-group bicapped tetrahedron model, P_6^{6+}, represented by **10**, which has 12 skeletal electrons. Figure 3 shows an idealized

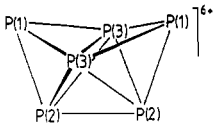

10

interaction diagram for **10**. The P_4 fragment on the left side of the Figure has T_d symmetry in which the $1b_2 + 1b_1 + 2a_1$ orbitals are the t_2 set and $1a_2 + 4a_1$ the e set. There are also four lone pairs that point away from the cluster ($3a_1 + 2b_2 + 5a_1 + 2b_1$). The orbitals for the $P\cdots P^{6+}$ capping unit are shown on the right side of the figure.

The capping Principle[3c] states that capping a face of a polyhedron makes no changes in the number of skeletal electrons because the three frontier orbitals of the capping unit are matched in symmetry by three low-lying orbitals of the uncapped polyhedron. Hence, the three framework orbitals in the polyhedron are stabilized and the three from the capping unit are greatly destablished. The same situation occurs in P_6^{6+}, resulting in the production of six framework orbitals and six lone pair orbitals, as shown in the diagram, although significant mixing occurs

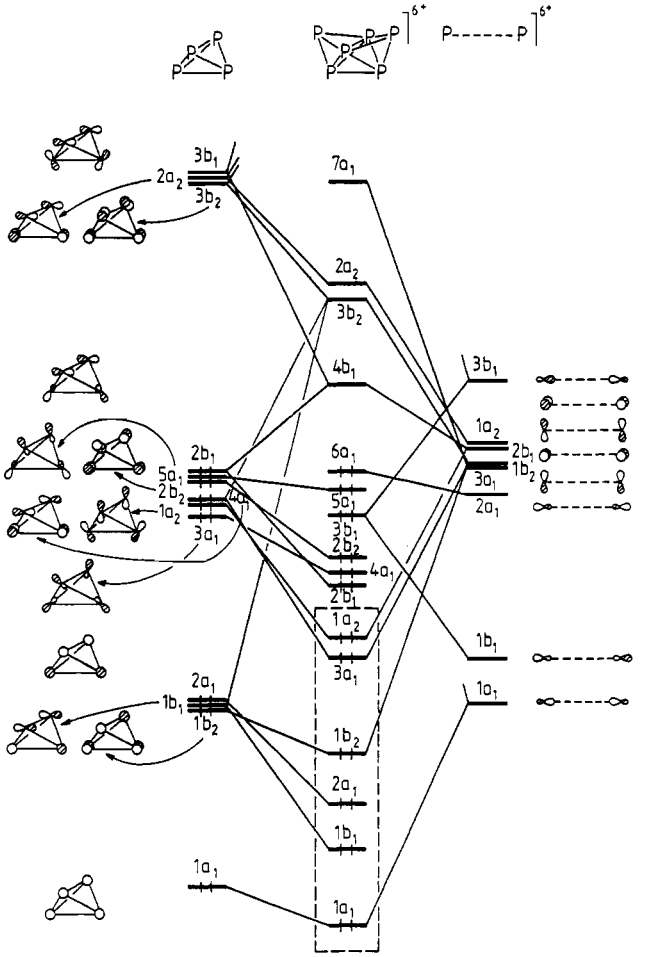

Figure 3. Idealized orbital interaction diagram for the bicapped tetrahedron P_6^{6+}. The dashed box encloses the orbitals responsible for the skeletal bonding.

between the framework and lone-pair orbitals. However, among the antibonding orbitals, three ($4b_1 + 3b_2 + 2a_2$) are kept at moderate energy by the empty ($3b_2 + 2a_2 + 3b_1$) set (t_1 in T_d symmetry) on P_4. This suggests that some bicapped tetrahedral clusters may be stable with six additional electrons.[49] The resultant shapes of the molecular $4b_1$, $2b_2$, and $2a_2$ orbitals are constructed in **11**–**13**. In each case the lower skeletal framework

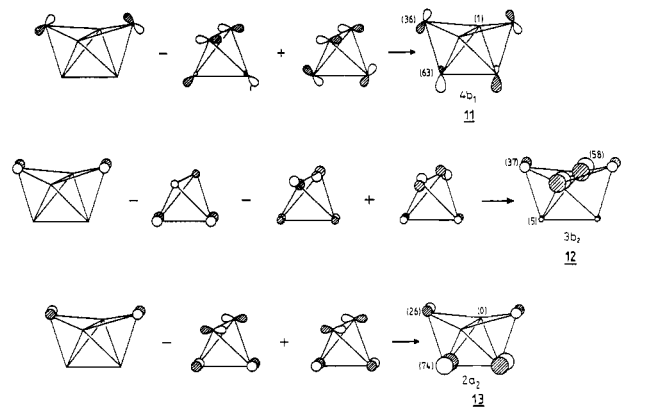

orbital mixes in an antibonding way to the capping orbital, while the upper orbital mixes in a bonding fashion. Notice that cancellation occurs on the P(3)–P(3) edge for the $4b_1$ and $2a_2$ MO's

(47) Halet, J.-F.; Saillard, J. Y. *J. Organomet. Chem.* **1987**, *327*, 365 and references therein.

(48) (a) Elian, M.; Chen, M. M. L.; Mingos, D. M. P.; Hoffmann, R. *Inorg. Chem.* **1976**, *15*, 1148. (b) Hoffmann, R. *Science* **1981**, *211*, 995. (c) Hoffmann, R. *Angew. Chem., Int. Ed. Engl.* **1982**, *21*, 711. (d) Stone, F. G. A. *Angew. Chem., Int. Ed. Engl.* **1984**, *23*, 89.

(49) Notice that with 14 skeletal electrons, the b_1 molecular orbital is the HOMO. For the P_6^{4+} cluster it is strongly antibonding along P(2)–P(2); see **11**. Thus, one would expect that lengthening this bond will stabilize the HOMO, which leads to a structure where two tetrahedral share an edge. This is in agreement with the principle of polyhedral condensation.[3]

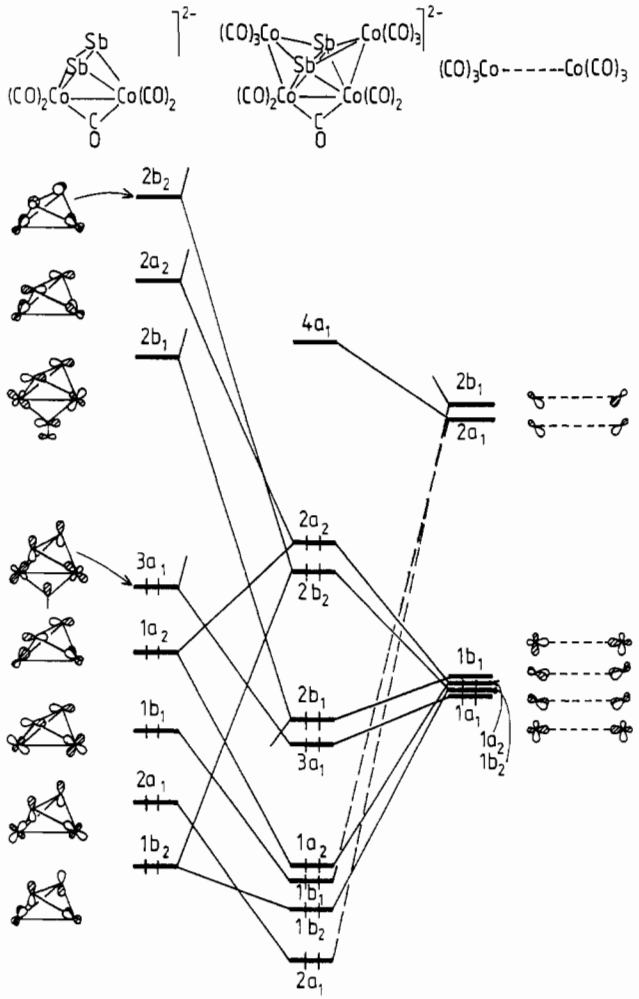

Figure 4. Orbital interaction diagram for the skeletal orbitals in $[\mathbf{2a}]^{2-}$. Notice that the lowest occupied orbital of a_1 symmetry (analogous to $1a_1$ in Figure 1) has not been included.

(**11**, **13**), while the coefficients on the P(2)–P(2) edge cancel in $2b_2$ (**12**), which is a result of the D_{5h} pseudosymmetry of a nido pentagonal bipyramid. For example, $2a_2$ can be viewed as the antisymmetrical component of the π-type e_2'' set of a regular P_5 pentagon and cannot mix by symmetry with the P(3)–P(3) fragment orbitals.

Figure 4 shows the orbital interaction diagram for $[Sb_2Co_4(CO)_{10}(\mu\text{-}CO)]^{2-}$ ($[\mathbf{2a}]^{2-}$). The important valence orbitals of the $[Sb_2Co_2(CO)_4(\mu\text{-}CO)]^{2-}$ tetrahedron are illustrated on the left side. A comparison with the orbitals of P_4 (Figure 3) reveals that $1b_2$, $2a_1$, and $1b_1$ correspond to the t_2 set in P_4, $1a_2$ and $3a_1$ corresponds to the e set and the $2b_1$, $2a_2$, and $2b_2$ levels strongly resemble the empty t_1 set in P_4. At low energy and not shown in Figure 4 is the skeletal orbital, which is fully bonding and is of a_1 symmetry. On the right side of this figure are the six valence orbitals of the $(OC)_3Co\cdots Co(CO)_3$ capping units. Again, there is a close correspondence between them and the $P\cdots P^{6+}$ capping units in Figure 3. The one difference is that now the $2a_1$ and $2b_1$ orbitals of the $(OC)_3Co\cdots Co(CO)_3$ caps are Co 4s and 4p in character, whereas the $1a_1$ through $1b_1$ combinations are comprised primarily of Co 3d.[1c] Consequently, the $2a_1$ and $2b_1$ levels energetically lie well above the others. Just like in the hypothetical P_6^{6+} cluster, six framework orbitals (five are shown in Figure 4) on the tetrahedral unit are stabilized by the caps. Furthermore, *three* molecular orbitals, labeled $2b_1$, $2b_2$, and $2a_2$, are kept at low energy because of the empty $2b_1 + 2a_2 + 2b_2$ set on the tetrahedron. Their composition is shown in **14**. There is one important difference between the two clusters. In P_6^{6+} the $2b_2$ molecular orbital (**12**) is actually concentrated on the P(3)–P(3) edge; however, the electronegativity difference between Co and Sb causes the electron density to mainly reside on the $Co(CO)_3$ caps. The

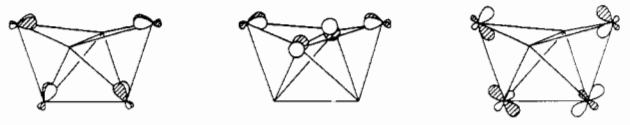

14

population of Sb_2 σ^* thus remains small, and as commented upon earlier, a substantial Sb–Sb interaction is retained in the molecule.

It is interesting to note that in $[\mathbf{2a}]^-$, $[\mathbf{2a}]^{2-}$, and $[\mathbf{2b}]^-$ the non-carbonyl-bridged Co–Co distances are always ~0.1–0.2 Å longer than that bridged by CO. The existence of a bridging carbonyl oftentimes obscures the extent of metal–metal bonding; however, computations on **8** (using equal Co–Co distances) indicate that the bridged bond is indeed stronger that the other two. The Co–Co overlap populations were 0.114 and 0.095, respectively. As previously mentioned, the principle structural change on going from $[\mathbf{2a}]^-$ to $[\mathbf{2a}]^{2-}$ is a 0.136 Å lengthening of the Co(2)–Co(3) bond. In our computations using the structural details associated with either molecule, we find the molecular orbitals labeled $2a_2$ and $2b_2$ in Figure 4 to be close in energy. Orbital a_2, however, in each instance lies at a higher energy. The $2a_2$ molecular orbital, shown in **14**, is Co(2)–Co(3) π (and δ) antibonding. Furthermore, it is substantially localized on Co(2) and Co(3); the relevant contributions are 60% Co(2)/Co(3), 12% Co(1)/Co(4), and 0.3% Sb(1)/Sb(2). Therefore, the addition of one electron to $2a_2$ on going from $[\mathbf{2a}]^-$ to $[\mathbf{2a}]^{2-}$ should indeed elongate the Co(2)–Co(3) bond. The computed overlap population drops from 0.066 in $[\mathbf{2a}]^-$ with $2a_2$ singly occupied to 0.026 with the addition of another electron but with maintenance of the geometry used for $[\mathbf{2a}]^-$.

Other Geometries and Related Cluster Systems. Finally, mention should be made of a trigonal-prismatic structure that is the one predicted by the Wade–Mingos rules[1-3] for 18 skeletal electron, six vertex clusters. Indeed several examples with this skeletal arrangement have been found.[50] Our calculations on trigonal-prismatic $Co_4(CO)_{12}(\mu_4\text{-}\eta^2\text{-}Bi_2)$ confirm that this structure is plausible at the 18 skeletal electron count (HOMO–LUMO gap = 1.56 eV). Our calculations are not reliable to predict an energy difference between it and the bicapped tetrahedral structure **8**; however, we note that in **8** the diffuse nature of the Bi atomic orbitals creates a greater stabilization with higher connectivity.

To summarize, there are several characteristics responsible for the 18 skeletal electron count of the E_2M_4 clusters considered here. The derivation from a nido pentagonal bipyramid points to the fact that four relatively electronegative M atoms should reside in the pentagonal plane and the two main group atoms at the apical positions. The bicapped tetrahedron derivation points to the requirement that the tetrahedral core must possess a low-lying set of three empty orbitals that are tangentially antibonding. This is likely to be met only when the skeletal orbitals of the tetrahedron are diffuse and do not overlap with each other strongly. Let us use these characteristics to examine other possible cluster types and skeletal isomers.

A 12 skeletal electron count (and not 18) is favored for one of the skeletal isomers of **8** shown in **15a**. The computed

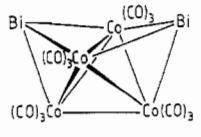

15a

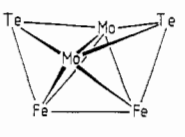

15b

HOMO–LUMO gap for this electron count is 0.86 eV. **15a** is not purely hypothetical, since the related 12 skeletal electron

(50) (a) Johnson, B. F. G.; Lewis, J.; Lodge, P. G.; Raithby, P. R.; Henrick, K.; McPartlin, M. *J. Chem. Soc., Chem. Commun.* **1979**, 719. (b) Field, J. S.; Haines, R. J.; Honrath, U.; Smit, D. N. *J. Organomet. Chem.* **1987**, *327*, C25. (c) For monocapped trigonal-prismatic M_4E_2 compounds, see: Gervasio, G.; Rossetti, R.; Stranghellini, P. L. *J. Chem. Soc., Chem. Commun.* **1977**, 387. Adams, R. D.; Wang, S. *J. Am. Chem. Soc.* **1987**, *109*, 924. Attali, S.; Dahan, F.; Mathieu, R. *J. Am. Chem. Soc.* **1988**, *110*, 1990.

$Cp_2Fe_2Mo_2(\mu_3\text{-}Te)_2(CO)_7$, shown in **15b**, adopts the same skeletal arrangement.[51] On the other hand, in P_6^{6+} (see Figure 3), there is a sizable b_1–b_2 HOMO–LUMO gap for a 14 electron count. However, occupation of the molecular b_1 level (analogous to **11** in the P_6^{6+} case) is expected to open the Co–Co bond in the pentagonal plane to form edge-shared tetrahedra. This is, in fact, the observed structure of the 14 skeletal electron $Cp_2Fe_2Mo_2(\mu_3\text{-}S)_2(CO)_8$.[52]

The bicapped tetrahedral geometry could be preserved for a 14 skeletal electron count (i.e., without breaking a bond) by reducing the antibonding interaction between the two in-plane atoms of the tetrahedron. This can be achieved by reducing the localization of the molecular orbital on these two atoms. This is what happens for **16a**, yet another skeletal isomer of **8**. Because

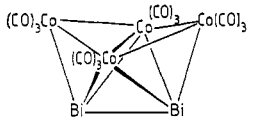

16a

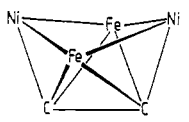

16b

of the electronegativity difference between Co and Bi, the $2b_1$ molecular orbital is now primarily localized on the capping Co atoms. As a result, the $2b_1$ level is low lying and a substantial gap occurs between $2b_1$ and $2b_2$ (0.98 eV) so that a 14 skeletal electron count should be possible. The $2b_2$–$2a_2$ (see Figure 4) energy difference in **16a** is also computed to be large. However, population of b_2 for a 16 skeletal electron count will break the Co–Co bond in the tetrahedral core. Just like in the P_6^{6+} system, molecular b_2 is localized on these two Co atoms and is strongly Co–Co antibonding. This is actually the structure observed for the 16-electron $Cp_2Ni_2Fe_2(CO)_6(\mu_4\text{-}\eta^2\text{-}C_2Ph_2)$ cluster[53] shown in **16b**.

A typical 12-electron bicapped tetrahedron that satisfies the Wade–Mingos electron-counting rules is $Os_6(CO)_{18}$ (**17**).[19] We

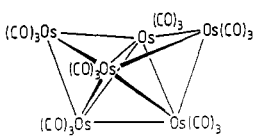

17

can ask the question of whether reduced variants of this cluster are possible while maintaining its structural integrity. We think not. The reason lies partly in the fact that the Os 5d orbitals are more diffuse and hence overlap with each other more than the Co 3d atomic orbitals. Consequently, the molecular a_2 and b_1 levels lies at a much higher energy than those shown in Figure 4. Likewise the a_2 molecular orbital is significantly destabilized by the lower lying "t_{2g}*-type" orbitals; see **6b**.

As mentioned previously, the bicapped tetrahedron derivation points to the fact the the tetrahedron may possess three low-lying "acceptor" orbitals. We have previously shown[29] that for a monocapped tetrahedron (trigonal bipyramid) of the E_4ML_3 type (where E = Bi) two members of the empty t_1 set can be used as acceptor orbitals. A 16 skeletal electron count is, therefore, possible. This situation was also anticipated by Teo and coworkers.[4a,b] In the bicapped tetrahedron all three members of the empty t_1 set are used; thus, clusters with 6 more skeletal electrons are possible. For a tricapped tetrahedron, **18**, the three members of the E_4 t_1 set are again used; furthermore, one symmetry-adapted linear combination of the M_3 set in **18** is left nonbonding.[29] Thus, a 20 skeletal electron count is possible and is in fact observed[29] in a derivative of $Bi_4Fe_3(CO)_9^{2-}$. For a tetracapped tetrahedron,

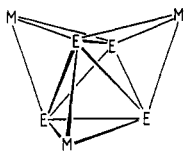

18

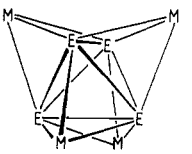

19

or stella quadrangula structure,[54] the four capping M units provide skeletal orbitals of $2t_2 + e + t_1 + a_1$ symmetry. Calculations on a hypothetical $[Bi_4Fe_4(CO)_{12}]^{2+}$ cluster reveal that the t_1 set on the Bi_4 tetrahedron do considerably stabilize the capping M_4 t_1 set. The primarily metal d, t_2 combination is *not* left nonbonding. Instead it overlaps reasonably well and is destabilized by the Bi_4 t_2 set of lone-pair orbitals. Consequently, we predict that the favored skeletal electron count for **19** to be 18 electrons.

A natural question arises concerning the electron count for a closo pentagonal bipyramidal cluster of M_5E_2 type. This closo structure can also be described as five almost regular tetrahedra sharing faces and having one common edge. Calculations on $Co_5(CO)_{15}(\mu_5\text{-}Bi)_2$ reveal that a 20 skeletal electron count is quite possible, i.e. four more electrons that the Wade–Mingos rules predict. The reason behind this is simple. We have already shown in Figure 2 that considering **7** or **8** as being a nido pentagonal bipyramid there are two additional electrons in a weakly antibonding orbital ($2a_2$). We have also shown that because of the pseudo-D_{5h} symmetry the $2a_2$ orbital can be considered to be one component of a π type e_2'' level that is localized on the pentagonal plane (see **13**). With five metal atoms in the pentagonal plane there now is a complete e_2'' set that is weakly antibonding and houses the additional four electrons. Johnston and Mingos have pointed out that deviations from the Wade–Mingos rules arise because bipolar clusters (such as the pentagonal bipyramid) do not possess a spherical field.[55]

Conclusions

Reaction of antimony halides with $Na[Co(CO)_4]$ provides an easy access into a series of antimony-containing cobalt carbonyl clusters. While the structural patterns observed for the products parallel those observed in the bismuth system, the reactivity patterns are surprisingly different. In both systems redox chemistry is observed leading to fragmentation and reorganization ultimately producing the structures $[\mathbf{2}]^{-/2-}$, which appear to be thermodynamically favored. A facile chemically and electrochemically reversible redox cycle relates these monoanion/dianion pairs with small changes in observed structural parameters. The most notable change appears to be in the CO-bridged Co–Co bond, which is found to be the molecular HOMO on the basis of both experimental and theoretical findings. Surprisingly, the paramagnetic monoanions are qualitatively more stable than the corresponding dianions.

Should the molecules considered in this study be regarded as nido pentagonal bipyramids or as bicapped tetrahedra? The metrical details of the structures provide no clear distinction, primarily because the tetrahedral angle (109.47°) is very close to the ideal pentagonal one (108°); i.e., a regular pentagonal bipyramid can be almost completely filled by packing together five regular tetrahedra. Our analysis of the electronic structure from both perspectives shows that each has its own merits. The pentagonal-bipyramidal derivation immediately shows why only one skeletal isomer is found for $[\mathbf{2a}]^-$ and $[\mathbf{2a}]^{2-}$. The bicapped tetrahedral derivation pinpoints the explanation why strong Bi–Bi and Sb–Sb bonding is retained in these clusters. It also implies that other capped main-group/transition-metal deltahedra will also provide exceptions to the classic electron-counting rule[1-5] for clusters.

(51) Bogan, L. E., JR.; Rauchfuss, T. B.; Rheingold, A. L. *J. Am. Chem. Soc.* **1985**, *107*, 3843.
(52) Braunstein, P.; Jud, J.-M.; Tiripicchio, A. *Angew. Chem., Int. Ed. Engl.* **1982**, *21*, 307.
(53) Sappa, E.; Manotti, Lanfredi, A. M.; Predieri, G.; Tiripicchio, A.; Carty, A. J. *J. Organomet. Chem.* **1985**, *288*, 365.
(54) For a discussion of the bonding in an infinite chain of flattened stella quadrangula, see: Zheng, C.; Hoffmann, R.; Nelson, D. R. *J. Am. Chem. Soc.*, in press.
(55) Johnston, R. L.; Mingos, D. M. P. *J. Chem. Soc., Dalton Trans.* **1987**, 647. The case of mixed main-group–transition metals with a dodecahedral framework has also been studied: Cox, D. N.; Mingos, D. M. P.; Hoffmann, R. *Ibid.* **1981**, 1788.

Note Added in Proof. Since this paper was submitted for publication, two new 84-electron, bicapped tetrahedral metal cluster complexes have been reported: $H_2Ru_6(CO)_{17}$ (McCarthy, D. A.; Krause, J. A.; Shore, S. G. *J. Am. Chem. Soc.* **1990**, *112*, 8587) and $Pt_2Os_4(CO)_{12}(COD)_2$ (Adams, R. D.; Wu, W. *Organometallics* **1991**, *10*, 35).

Acknowledgment. K.H.W. thanks the Robert A. Welch Foundation and the National Science Foundation for support and Dr. Graham Palmer (Rice University) for providing the ESR spectra. T.A.A. thanks the donors of the Petroleum Research Fund, administered by the American Chemical Society, the Robert A. Welch Foundation, and the National Science Foundation (for a grant of supercomputer time at the Pittsburgh Supercomputing Center). J.-Y.S. and J.-F.H. thank the CNRS for financial support.

Supplementary Material Available: Tables of atomic coordinates, anisotropic displacement parameters, full crystallographic data collection parameters, and bond angles and distances for [PPN][**2a**], $[PPN]_2$[**2a**], and $[Cp_2Co]$[**2b**] and ORTEP diagrams for [PPN][**2a**] and $[Cp_2Co]$[**2b**] (18 pages); listings of observed and calculated structure factors (52 pages). Ordering information is given on any current masthead page.

Contribution from the Department of Chemistry, Faculty of Science, Kyushu University 33, Hakozaki, Higashi-ku, Fukuoka 812, Japan

Preparation and Redox Chemistry of Novel Carbonato-Bridged Cobalt(II) Complexes with 1,4,8,11-Tetrakis(2-aminoethyl)-1,4,8,11-tetraazacyclotetradecane and 1,4,8,11-Tetrakis(pyridylmethyl)-1,4,8,11-tetraazacyclotetradecane

Hirotaka Harada, Masahito Kodera,* Gordana Vučković, Naohide Matsumoto, and Sigeo Kida*

Received June 1, 1990

Carbonato-bridged binuclear cobalt(II) complexes with 1,4,8,11-tetrakis(2-aminoethyl)-1,4,8,11-tetraazacyclotetradecane (taec), $[Co_2CO_3(taec)](ClO_4)_2 \cdot 2H_2O$ (**1a**) and $[Co_2CO_3(taec)]X_2 \cdot NaX \cdot H_2O$ (X = ClO_4 (**1a'**) and BF_4 (**1b**)), and with 1,4,8,11-tetrakis(pyridylmethyl)-1,4,8,11-tetraazacyclotetradecane (tpmc), $[Co_2CO_3(tpmc)]X_2 \cdot 2H_2O$ (X = ClO_4 (**2a**) and BF_4 (**2b**)), were prepared and characterized by IR and electronic spectra, magnetic susceptibility and cyclic voltammetry. Complex **1a'** has been structurally characterized by X-ray crystallography. It crystallizes in the space group $P2_1/a$ with a = 26.419 (10) Å, b = 12.774 (5) Å, c = 10.410 (3) Å, β = 90.51 (4)°, V = 3513 Å^3, Z = 4 and ρ_{calcd} = 1.72 g/cm^3. The structure was refined by full-matrix least-square techniques to a final R factor of 0.068 and R_w factor of 0.057 for 3582 data with $|F_o| > 3.0\sigma(|F_o|)$. The complex can be described in terms of distorted-octahedral geometry. That is unique among the taec complexes in taking six-coordination owing to the special bridging structure of CO_3^{2-}. Cyclic voltammograms of the cobalt complexes were compared with five-coordinated cobalt complexes $[Co_2OH(taec)](ClO_4)_3$ (**1c**) and $[Co_2OH(tpmc)](ClO_4)_3$ (**2c**) and revealed that the six-coordinated structure lowered the redox potential for oxidation of cobalt(II) to cobalt(III). Air oxidation of **1a** and **1b** in aqueous solution produced a cobalt(III) complex that was detected by characteristic absorption at 364 and 532 nm. The spectral, magnetic, and elemental analysis data demonstrated that the oxidized product isolated was a mixed-valence $Co^{III}Co^{II}$ complex.

Introduction

In the series[1] of investigations on octaamine ligands 1,4,8,11-tetrakis(2-aminoethyl)-1,4,8,11-tetraazacyclotetradecane (taec) and 1,4,8,11-tetrakis(pyridylmethyl)-1,4,8,11-tetraazacyclotetradecane (tpmc) Kida and co-workers reported that $[Co_2OH(taec)](ClO_4)_3$ (**1c**[2]) is usually stable against chemical and electrochemical oxidation. This was attributed to the steric hindrance of methylene groups[3] of the ligand for attaining six-coordination of cobalt. It was also shown that the chromium(II) oxidation state is stabilized in $Cr_2(taec)X_4$ (X = Cl, Br)[4] for the same reason. In the continuing efforts to obtain new complexes of taec and tpmc, $[Ni_2CO_3(taec)](ClO_4)_2$[5] was found to have distorted octahedral coordination caused by the novel bridging structure[6] of carbonate ion[7] as depicted in Figure 1.

Recently, we prepared a carbonato-bridged cobalt(II) complex with a tricyclic octaamine ligand derived from cyclam and partially reported the cyclic voltammetry of the complex.[17] The redox potential for the Co(II)/Co(III) process of the complex certainly decreased, compared with that of the hydroxo-bridged cobalt(II) complex of the tricyclic ligand. The cause of the stabilization of Co(III) state, however, was not investigated in detail, and isolation of the oxidized Co(III) complex was not attained.

Thus, in this study, we aimed to obtain six-coordinate cobalt(II) complexes with taec and tpmc, expecting them to undergo much more facile oxidation to cobalt(III).

Experimental Section

Safety Note. *Caution!* Perchlorate salts of metal complexes with organic ligands are potentially explosive. Only small amounts of material should be prepared, and these should be handled with great caution.

Preparations. $Co(ClO_4)_2 \cdot 6H_2O$ was prepared from basic cobalt(II) carbonate (Nacalai Tesque, reagent grade).[8a] $Co(BF_4)_2 \cdot 6H_2O$ was obtained in a manner similar to that used for the perchlorate except that aqueous HBF_4 was used instead of $HClO_4$. The ligands, taec[1a] and tpmc,[8b] were prepared by the literature methods.

$[Co_2CO_3(taec)](ClO)_2 \cdot 2H_2O$ (1a). All procedures were carried out under an argon atmosphere in a Schlenk apparatus. To an aqueous solution (5 mL) containing taec (500 mg, 1.34 mmol) and Na_2CO_3 (144 mg, 1.34 mmol) was added $Co(ClO_4)_2 \cdot 6H_2O$ (1.008 g, 2.75 mmol) with stirring. The solution was stirred for 5 min. The resultant precipitates were removed by filtration, and the filtrate was concentrated to 2 mL. To the solution was added 5 mL of degassed ethanol, and the resultant solution was allowed to stand for 12 h. Purple crystals were formed, which were collected by filtration, washed with a small amount of cold water and dried in vacuo over P_2O_5. Yield: 530 mg (50.3%). **1a** could be recrystallized from water/ethanol to form microcrystals, but it was difficult to prepare crystals suitable for X-ray crystal structure analysis. Anal. Calcd for $C_{19}H_{48}N_8Cl_2O_{13}Co_2$: C, 29.05; H, 6.16; N, 14.26; Co, 15.01. Found: C, 29.32; H, 6.00; N, 14.29; Co, 14.23. IR (KBr pellet): 3440, 3250, 2860, 1560, 1460, 1330, 1150-1030, 990, 965, 900, 865, 840, 815, 755, 630 cm^{-1}. UV-vis (H_2O) λ_{max}, nm (ϵ): 504 (53), 552 (48).

(1) (a) Murase, I.; Mikuriya, M.; Sonoda, H.; Fukuda, Y.; Kida, S. *J. Chem. Soc., Dalton Trans.* **1986**, 953. (b) Murase, I.; Mikuriya, M.; Sonoda, H.; Kida, S. *J. Chem. Soc., Chem. Commun.* **1984**, 692. (c) Kida, S.; Murase, I.; Harada, C.; Daizeng, L.; Mikuriya, M. *Bull. Chem. Soc. Jpn.* **1986**, *59*, 2595. (d) Mikuriya, M.; Kida, S.; Murase, I. *J. Chem. Soc., Dalton Trans.* **1987**, 1261. (e) Mikuriya, M.; Kida, S.; Murase, I. *Bull. Chem. Soc. Jpn.* **1987**, *60*, 1355. (f) Mikuriya, M.; Kida, S.; Murase, I. *Bull. Chem. Soc. Jpn.* **1987**, *60*, 1681.
(2) Mikuriya, M.; Kida, S.; Kohzuma, T.; Murase, I. *Bull. Chem. Soc. Jpn.* **1988**, *61*, 2666.
(3) Szalda, D. J.; Fujita, E.; Creutz, C. *Inorg. Chem.* **1989**, *28*, 1446.
(4) Asato, E.; Kida, S.; Murase, I. *Inorg. Chem.* **1989**, *28*, 800.
(5) Mikuriya, M.; Murase, I.; Asato, E.; Kida, S. *Chem. Lett.* **1989**, 497.
(6) (a) Churchill, M. R.; Davies, G.; El-Sayed, M. A.; El-Shazly, M. F.; Hutchinson, J. P.; Rupich, M. W.; Watkins, K. O. *Inorg. Chem.* **1979**, *18*, 2296. (b) Churchill, M. R.; Davies, G.; El-Sayed, M. A.; Hutchinson, J. P. *Inorg. Chem.* **1982**, *21*, 1002. (c) Davies, A. R.; Einstein, F. W. B. *Inorg. Chem.* **1980**, *19*, 1203.
(7) (a) Mac-coll, C. R. P. *Coord. Chem. Rev.* **1969**, *4*, 147. (b) Churchill, M. R.; Lashewycz, R. A.; Koshy, K.; Dasgupta, T. P. *Inorg. Chem.* **1981**, *20*, 376.
(8) (a) Kiss, A. v.; Gerendas, M. *Z. Phys. Chem.* **1937**, *A180*, 117. (b) Alcock, N. W.; Balakrishnan, K. P.; Moore, P. *J. Chem. Soc., Dalton Trans.* **1986**, 1743.

0020-1669/91/1330-1190$02.50/0